Inorganic Chemistry

Article

pubs.acs.org/IC

Remarkable Inertness of Copper(II) Chelates of Cyclen-Based Macrobicycles with Two *trans*-*N*-Acetate Arms

Catarina V. Esteves,[†] Pedro Lamosa,[†] Rita Delgado,*[,†] Judite Costa,[‡] Pauline Désogère,[§] Yoann Rousselin,[§] Christine Goze,[§] and Franck Denat*[,§]

[†]Instituto de Tecnologia Química e Biológica, Universidade Nova de Lisboa, Av. da República, 2780-157 Oeiras, Portugal

[‡]iMed.UL, Faculdade de Farmácia, Universidade de Lisboa, Av. Prof. Gama Pinto, 1649-003 Lisboa, Portugal

[§]Institut de Chimie Moléculaire de l'Université de Bourgogne, UMR CNRS 6302, Université de Bourgogne, 9, Av. Alain Savary, 21078 Dijon, France

Supporting Information

ABSTRACT: Two cross-bridged cyclen-based macrocycles with two *trans*-*N*-acetic acid arms, one having a dibenzofuran (DBF) moiety as the bridge, H_2L1, and the other a diphenyl ether (DPE) one, H_2L2, were synthesized. Both compounds behave as "proton sponges." The thermodynamic stability constants for the Cu^{2+}, Zn^{2+}, Al^{3+}, and Ga^{3+} complexes of both compounds were determined. They exhibit an excellent thermodynamic selectivity for copper(II), ensuring that metal ions largely present in the human body do not interfere with the copper(II) chelates. All complexes are very slow to form, and [CuL2] and [CuL1] are extremely inert to demetallate, especially [CuL2]. The acid-assisted dissociation of [CuL1] led to a half-life of 4.28 h in 5 M HCl at 363.2 K, while [CuL2] needed harsher conditions of 12 M HCl at 363.2 K with a half-life of 30.8 days. To the best of our knowledge, [CuL2] exhibits the highest half-life value for a copper(II) complex of a polyazamacrocycle derivative reported in the literature until now. Single crystal X-ray diffraction determined for $[Cu(H_2L1)](ClO_4)_2$ showed the copper center in a distorted octahedral environment bound to the N_4O donors of the macrobicycle and one oxygen atom from a carboxylic arm, while for [CuL2] it showed the copper center in a trigonal bipyramid geometry only bound to the donors of the macrobicycle and leaving the carboxylate arms away from the coordination sphere. UV−vis−NIR and X-band EPR spectra showed that in [CuL1] the copper center adopts a distorted compressed octahedral environment, which is the only structure found in solution for this complex, while in [CuL2] a similar environment was found in the first stages of its slow formation but reached a square-pyramidal geometry upon stabilization. The acetate arms play therefore an important role during the formation of the complex, as revealed by the comparison of its complexation behavior with the corresponding parent compounds.

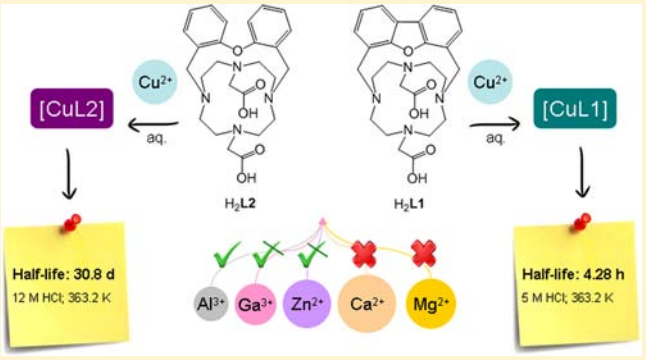

INTRODUCTION

Tetraazamacrocycles and their many derivatives have an excellent ability to form stable complexes with a large scope of metal ions; therefore their study continues to raise huge interest among researchers.[1−6] The high thermodynamic stability and kinetic inertness of metal complexes of some *N*-functionalized derivatives of tetraazamacrocycles, especially cyclen (cyclen = 1,4,7,10-tetraazacyclododecane) and cyclam (cyclam = 1,4,8,11-tetraazacyclotetradecane), make such chelates useful for medical applications in clinical imaging and therapy. A large number of cyclen and cyclam derivatives have been prepared with functionalized substituents such as carboxylic acids, phosphonic acids, phosphinic acids, amines, amides, alcohols, pyridyl, and more recently a combination of different substituents in the same molecule.[1,2,4−7] Some of them were explored as contrast agents for magnetic resonance imaging (MRI) using Gd^{3+} complexes[8−12] and others in nuclear medicine for radioimmunotherapy using several radiolanthanide chelates,[13−16] upon conjugation to suitable biomolecules for target-specific delivery to organs or tissues in patients.[17]

In order to avoid metal transchelation into the living body, more rigid compounds derived from cyclen or cyclam have been investigated, currently known as constrained or reinforced macrocycles. In these compounds an alkylene bridge is covalently bound to two opposite nitrogen atoms, ethylene or propylene chains are the most common, and the compounds are known as cross-bridged compounds, adamanzanes, or cryptands.[18−26] The cross-bridged compounds adopt conformations where all four nitrogen lone pairs point to inside the cavity upon protonation or metal chelation. The small cavity generated and the number of donor atoms particularly

Received: January 7, 2013
Published: April 11, 2013

   dx.doi.org/10.1021/ic400015v | Inorg. Chem. 2013, 52, 5138−5153

favors the coordination of the Cu^{2+} metal ion, especially when two additional arms are bound to the other two *trans-N* amines, such as acetate, methylphosphonate, methylamide, etc. In general, they are remarkably efficient "proton sponges."[18−26] Due to the geometric configuration of these compounds, their copper(II) complexes exhibit slow formation and inertness to dissociation. These features place these copper(II) chelates as the best candidates for radiopharmaceutics using ^{67}Cu for therapeutic purposes or ^{64}Cu for positron emission tomography (PET).[27−34] The main drawback of these chelators for the preparation of radiochelates is their slow kinetic formation, thus needing heating which is not compatible with labeling of sensitive biomolecules (antibodies, enzymes, etc.).

In this context we decided to prepare and study two cross-bridged derivatives of cyclen, containing unusual and longer bridges bound to the 1,7-positions of cyclen, such as a dibenzofuran, DBF, and diphenylether, DPE, moieties (H_2L1 and H_2L2, see Chart 1). Both compounds have additional *N*-acetate arms bound to the 4,10-positions of the macrocycle. The parent macrobicycles (L3 and L4) were already studied by some of us,[35] including some of their metal complexes.[36] They also behave as "proton sponges," and their complexes with Cu^{2+} and Zn^{2+} were very difficult to form and could not be prepared in aqueous solution but in acetonitrile. The introduction of the two acetate arms changes dramatically their metal complexation behavior and improves their solubility in water. In this work, the acid−base reactions of H_2L1 and H_2L2 were studied as well as their coordination properties with Cu^{2+}, Zn^{2+}, Al^{3+}, and Ga^{3+} ions in solution and in the solid state.

Chart 1. Structures of Compounds Discussed in This Work

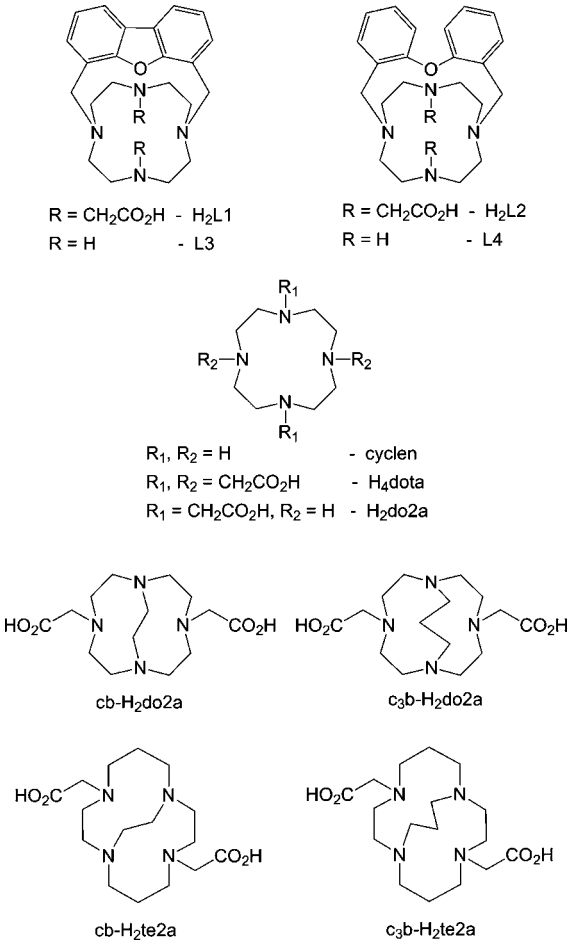

RESULTS AND DISCUSSION

Syntheses of the Compounds. The parent macrobicyclic compounds were synthesized before,[35,36] and the additional *trans*-acetate arms were introduced by reaction with *tert*-butyl bromoacetate at 40 °C in CH_3CN followed by deprotection in concentrated hydrochloric acid, see Scheme 1.

Scheme 1. Synthetic Procedures[a]

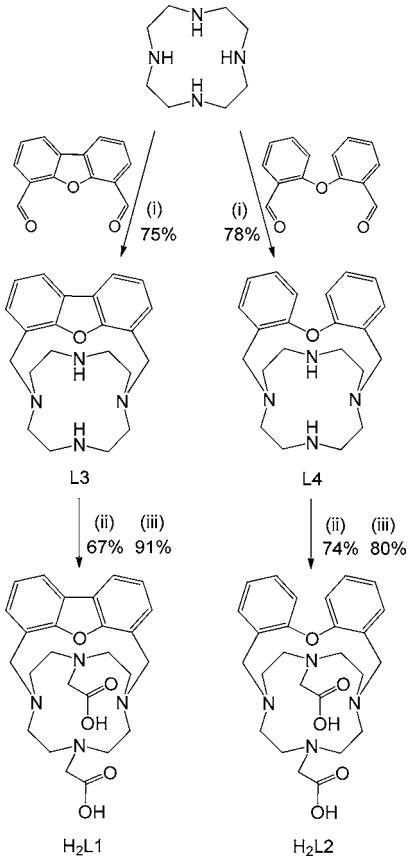

[a]Reagents and conditions: (i) 2.8 equiv. $NaBH(OAc)_3$, dichloroethane, N_2, room temperature, 2 d; (ii) 2.2 equiv. ^{t}butylbromoacetate, 4 equiv. K_2CO_3, CH_3CN, 40 °C, 4 h; (iii) HCl, room temperature, 10 min.

Acid−Base Behavior of the Cross-Bridged Compounds, H_2L1 and H_2L2. *Potentiometric Measurements.* Both compounds have six basic centers, four amines and two carboxylates, from which only three protonation constants were possible to obtain by potentiometric data in aqueous solutions, where reliable pH values are only available at the 2.5−11.5 range. The first protonation value was determined by spectrophotometric titrations. ^{1}H NMR titrations were also undertaken at 6.5−14.5 pD values aiming the determination of K_1^H but without success, see below. All the potentiometric and spectrophotometric measurements were carried out at 298.2 ± 0.1 K in aqueous solution and at an ionic strength of 0.10 ± 0.01 M in $N(CH_3)_4NO_3$. The stepwise protonation constants (K_i^H) obtained are compiled in Table 1, together with the values for the parent macrocycles,[36] cyclen,[37−40] H_2do2a,[41] and H_4dota[42,43] for comparison. Overall protonation constants

dx.doi.org/10.1021/ic400015v | Inorg. Chem. 2013, 52, 5138−5153

Table 1. Stepwise Protonation (K_i^H) Constants of H_2L1 and H_2L2 Compounds, the Parent Cryptands, Cyclen, H_2do2a, and H_4dota (T = 298.2 K, I = 0.10 M in $N(CH_3)_4NO_3$)

equilibrium reaction	H_2L1	H_2L2	L3	L4	cyclen	H_2do2a	H_4dota
$L + H^+ \rightleftarrows HL$	15.0[a]	14.6[a]	>12[b]	11.53[b]	11.27[c]	11.45[d]	12.09[e]
$HL + H^+ \rightleftarrows H_2L$	9.59[f]	8.86[f]	8.97[b]	9.05[b]	9.96[c]	9.54[d]	9.76[e]
$H_2L + H^+ \rightleftarrows H_3L$	2.33[f]		2.70[b]	2.63[b]	2.18[c]	4.00[d]	4.56[e]
$H_3L + H^+ \rightleftarrows H_4L$	1.7[f]				1.74[c]	2.36[d]	4.09[e]
$H_2L + 2\ H^+ \rightleftarrows H_4L$	4.0[f]	5.05[g]			3.92	6.36	
$L + 4\ H^+ \rightleftarrows H_4L$	28.6	28.5	>23.7	23.21	25.15	27.35	30.50

[a]This work, determined by spectrophotometric titration. [b]T = 298.2 K, I = 0.1 M in $N(CH_3)_4Cl$.[36] [c]T = 298.2 K, I = 0.5 M in KNO_3.[37] Slightly different values were found by other authors: T = 298.2 K, I = 0.1 M in $NaNO_3$, log K_1 = 10.6, log K_2 = 9.6, log K_3 < 2, log K_4 < 2;[38] T = 298.2 K, I = 0.10 M in $NaClO_4$, log K_1 = 11.04, log K_2 = 9.86, log K_3 < 2, log K_4 < 2;[39] and T = 298.2 K, I = 1 M in NaCl, log K_1 = 10.7, log K_2 = 9.7, log K_3 = 1.73, log K_4 = 0.94.[40] [d]T = 298.2 K, I = 0.10 M in $N(CH_2CH_3)_4NO_3$.[41] [e]T = 298.2 K, I = 0.10 M in $N(CH_3)_4NO_3$.[42,43] [f]This work, determined by potentiometric titration. [g]The values of log K_3 and log K_4 are on the same order; the system converges with better statistic parameters for a value of the global constant (including K_3 and K_4) of 5.05, which is about 2.5 for each stepwise constant.

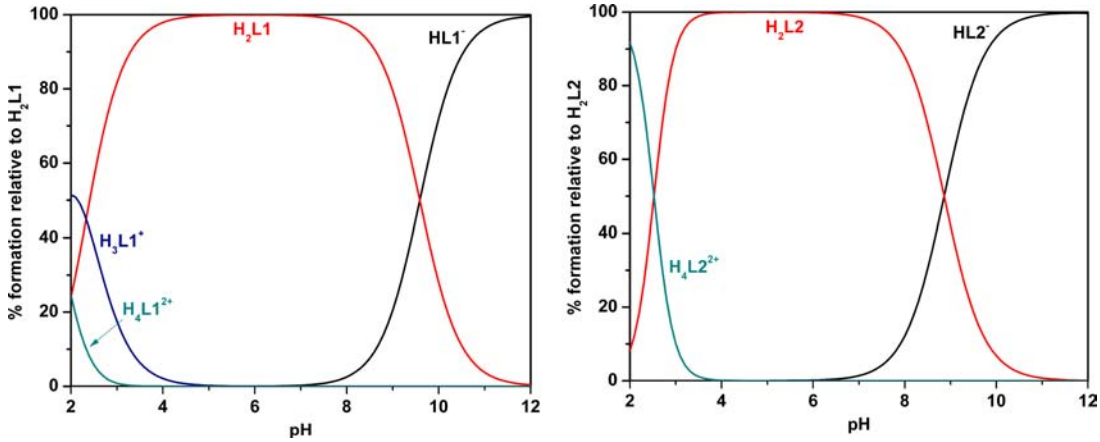

Figure 1. Species distribution diagrams of H_2L1 (left) and H_2L2 (right) in aqueous solution at $c_L = 1.0 \times 10^{-3}$ M.

(β_i^H) with standard deviations are collected in Table S1 in the Supporting Information. In Figure 1 are represented the species distribution diagrams of H_2L1 and H_2L2 as a function of the pH.[44] These diagrams show the very similar behavior of both compounds along the pH, the neutral species H_2L being the main one from pH 3 to about 8, and the completely deprotonated species L^{2-} does not start to form even at pH 12.

Depending of the functional group of the arms, all *N*-substituted cyclen derivatives possess two high protonation constants and the others low or very low. Moreover, most of the cross-bridged compounds behave as "proton sponges," having the first protonation constant particularly high.[45] The first two values correspond to the protonation of nitrogen atoms inside the macrocyclic cavity in opposite positions, eventually forming $^+$N−H···N hydrogen bonds.[36,45,46] For cyclen, the other two values correspond to the protonation of the other two amines of the ring, and the resulting strong repulsions led to the very small values. In *N*-acetate cyclen derivatives, when the protonation occurs in the arms bound to nonprotonated amines, the log values are >4, as in acetic acid (and also found for the H_4dota).[42,43] On the other hand, when the protonation occurs at the acetate arm bound to a protonated amine the value is much lower (≤2.5, as for amino acids) and can occur simultaneously with partial protonation of the last two amines of the macrocycle.[41,43,47] On the basis of these data, it is possible to predict that the first two protonations in H_2L1 and H_2L2 occur mainly on the amines carrying the acetate arms and the next two on the acetate arms, see ^{1}H NMR titrations below.

Spectrophotometric Measurements. The present compounds, as other cross-bridged ones, were found to be "proton sponges."[45] Macrobicycles of short bridges (ethylene and propylene) when protonated adopt a conformation having the four nitrogen lone pairs convergent to the center of the cavity with the protons involved in a network of strong $^+$N−H···N hydrogen bonds. In such cases, the completely deprotonated species is not observed in aqueous solution, and therefore the first protonation constant (K_1^H) cannot be determined by usual potentiometric measurements. In this work, the K_1^H values of both compounds were determined by spectrophotometric titrations, using very concentrated solutions of KOH as the titrant, see Figure 2 for H_2L2 and Figure S1 of the Supporting Information for H_2L1. In fact, by ^{1}H NMR in D_2O no shift of proton resonances was observed at pD > 11, and consequently, it was not possible to determine the K_1^H but only the K_2^H values, those that were also possible to determine by the potentiometric data.

NMR Measurements. The ^{1}H NMR titrations in D_2O showed some important differences in the structural behavior of the two compounds derived from the specific architecture of each bridge. The titration of both compounds was carried out at pD values >6.

The assignment of the NMR signals of H_2L1 was done at 308.2 K and pD 7.48 and 13.78 (see Table S2 of Supporting Information), on the basis of 1D and 2D spectra (COSY, HSQC, and HMBC). The downfield region of the proton modulated carbon spectrum of this compound (APT) displays seven signals, four of which correspond to quaternary carbon

dx.doi.org/10.1021/ic400015v | Inorg. Chem. 2013, 52, 5138−5153

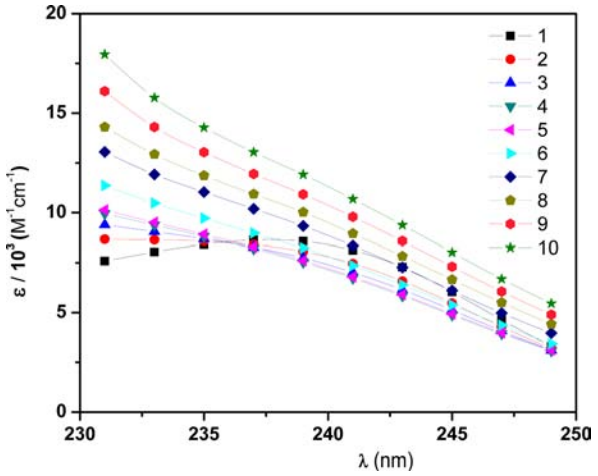

Figure 2. UV titration of H_2L2 for the determination of the first two protonation constants, at 298.2 K using 10 selected wavelengths. Increased amount of titrant KOH added from **1** to **10**.

atoms. The correlations found in the HSQC spectrum led to the identification of the signals of the protons linked to the other three carbon atoms. The sequential information from the COSY spectrum together with the 2 to 3 bond distance information taken from the HMBC spectrum allowed unequivocal assignment of all of the aromatic resonances (see Table 2). Moreover, the HMBC spectrum showed unique correlations between the aromatic signals and a resonance at 57.0 ppm in the ^{13}C spectrum, allowing the assignment of the aliphatic carbon of the bridge (see Figures S2−S5 in Supporting Information). A similar reasoning allowed the assignment of a broad signal centered at 3.05 ppm in the proton spectrum to the CH_2 of the acetate groups. The resonances due to the cyclen ring were assigned also using the HMBC spectrum: there were correlations between the bridge and the carbon atom at position 8 (see numbering scheme in Figure 3) and between the acetate arms and positions 8 and 9. It is curious to notice that there are two different proton resonances at position 9; this is probably due to the hydrogen atoms above or below the plane of the cyclen ring. However, this effect is not visible on the protons at position 8, whose signals appear as a singlet.

The assignment of the ^1H and ^{13}C resonances of H_2L2 was performed at 313.2 K and pH 7.17 (and at pH 13.89, see Table S2) and followed the same reasoning resorting to the COSY and HSQC spectra and taking into consideration the 2 to 3 bond distance information of the HMBC. In H_2L2, the geometry of the bridge probably forces the planes of the benzene rings to tilt toward the cyclen plane in opposite directions. This conformation, while preserving the symmetry of the bridge, distorts the symmetry of the cyclen ring. This causes the protons at position 7 to resonate at very different chemical shifts due to the different ring current shifts arising from the different angles adopted in respect to the planes of the aromatic rings (see Table 2) and also the carbon atoms at positions 8 and 9 on either side of the ring to be distinguishable. Differences between the hydrogen atoms above or below the plane of the cyclen ring are also observable, see Figure 4.

For H_2L1, when the equilibrium $H_2L1 \rightleftarrows HL1^- + H^+$ occurs (9.39 to 10.95 pD region), for each amount of KOD added the signals of all proton resonances decrease in intensity, and upfield shifted signals of increasing intensity appear, indicating the slow exchange of the equilibrium compared to the NMR relaxation time, see Figure 3. Additionally, it was observed that with the change of the pH, all protons (of the cyclen ring, the acetate arms, and the bridge) exhibit shifts of comparable magnitude. This feature can have two explanations: (a) the proton involved is shared by the four amine centers or/and (b) the deprotonation causes a conformational change which leads to a different orientation of the planes of the aromatic rings located on the bridge, with the consequent difference of the magnitude of the ring current shifts felt by all of these protons. In this last scenario, the effect of the current shifts will obscure the chemical shift changes caused directly by the deprotonation, making it impossible to say, from the NMR data, which of the nitrogen atoms is being deprotonated. Moreover, with these data it was also possible to determine the value of $K_2^{D_2O}$, using the ratio of areas between the decreased first signal and the corresponding increased one of the new species, which is log $K_2^{D_2O}$ = 9.92, see Figure 5. The conversion of this value to the corresponding constant in water gives log $K_2^{H_2O}$ = 8.9[48] and 9.3,[49] which are values only slightly lower than the more accurate one determined by potentiometric measurements. For this compound, it was not possible to perceive the

Table 2. ^1H and ^{13}C Resonance Assignment of Compounds H_2L1 (at pD = 7.48) and H_2L2 (at pD = 7.17)

	H_2L1/δ (ppm)		H_2L2/δ (ppm)	
position[a]	^{13}C	^1H	^{13}C	^1H
1	153.2		154.9	
2	121.7		120.3	7.09 (d, ^3J = 8.2 Hz)
3	121.8	8.21 (d, ^3J = 7.6 Hz)	130.4	7.50 (t, ^3J = 7.5 Hz)
4	124.2	7.53 (t, ^3J = 7.5 Hz)	124.6	7.36 (t, ^3J = 7.2 Hz)
5	129.2	7.57 (d; ^3J = 7.3 Hz)	133.1	7.57 (d, ^3J = 7.3 Hz)
6	124.3		127.3	
7	57.0	4.28 (s)	53.5	5.08−5.04; 3.44−3.37
8	48.6	3.14−3.12	47.8	3.59−3.48; 2.98−2.92
8′			47.2	3.19−3.12; 2.88−2.82
9	53.8	3.95−3.93; 3.47−3.43	51.3	4.22−4.15;3.61−3.53
9′			51.3	3.61−3.53; 3.42−3.25
10	50.6	3.08−3.01	54.7	3.20−3.17
11	168.6		168.5	

[a]See Figures 3 and 4 for numbering of the atoms.

dx.doi.org/10.1021/ic400015v | Inorg. Chem. 2013, 52, 5138−5153

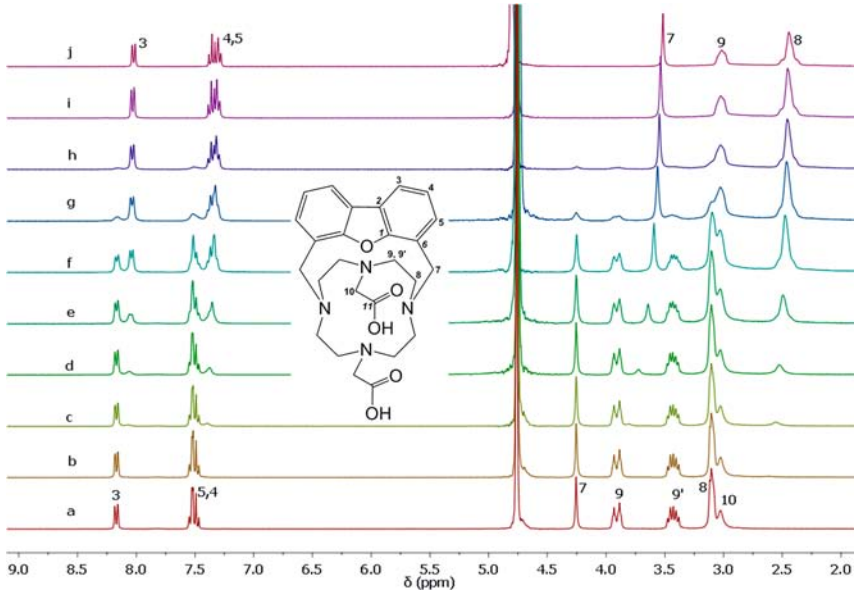

Figure 3. ^{1}H NMR spectra of H_2L1 in D_2O at different pD values and the structure of the compound with numbering of atoms. The pD values are a, 8.23; b, 8.89; c, 9.39; d, 9.67; e, 9.92; f, 10.20; g, 10.60; h, 10.95; i, 12.23; j, 14.39.

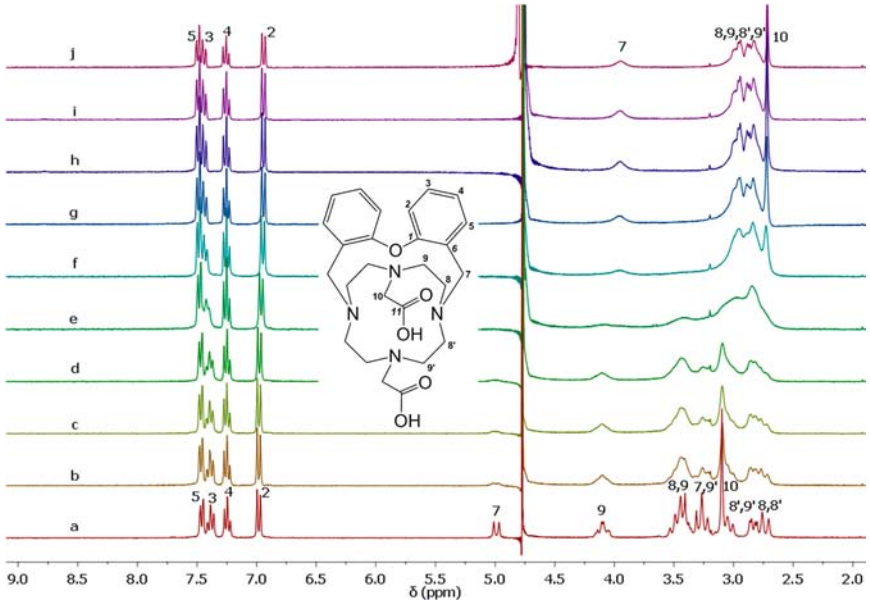

Figure 4. ^{1}H NMR spectra of H_2L2 in D_2O at different pD values and the structure of the compound with numbering of atoms. The pD values are a, 7.34; b, 8.58; c, 8.84; d, 9.05; e, 9.86; f, 10.58; g, 11.22; h, 12.13; i, 13.14; j, 14.35.

deprotonation start of the last proton, even at pD ≈ 14. This proton should be very well accommodated into this rigid bridged cyclen cavity probably forming bifurcated $^{+}$N−H···N hydrogen bonds with all the other nitrogen atoms, as the resulting ^{1}H NMR spectrum of this species presents only three resonances at the upfield region and two resonances downfield.

For the compound H_2L2, some of the proton resonances are difficult to follow with pD, especially for the cyclen aliphatic signals (Figure 4). The protons 7 at 5.0 and 3.4 ppm collapse into a broad signal around 4 ppm. The protons at positions 9 and 10 that are detached from the other cyclen aliphatic protons showed a strong downfield shift, indicating the nitrogen bearing the acetate arm as the likely site of this deprotonation, an observation in accordance with the potentiometric pK_a values. For the aromatic signals, no significant shift with the pD was observed for protons 5 and 4, while protons 3 and 2 move slightly, and in opposite directions, see Figure S6. One must highlight that between 8.58 < pD < 9.86 all aliphatic peaks are broad, which can be related to the existence of the second protonation constant and an intermediate exchange rate between the various differently protonated species in respect to the NMR time. On the basis of shifts of only 3, 7, and 10 proton resonances, the value obtained for the corresponding log $K_2^{D_2O}$ = 9.86. The conversion of this value to the corresponding constant in water gives log $K_2^{H_2O}$ = 8.86[48] and 9.21,[49] which are in good agreement with the one determined by potentiometric measurements.

Complexation Studies. The ability to form thermodynamically and kinetically stable metal complexes with H_2L1 and H_2L2 was also investigated, and in some cases the

dx.doi.org/10.1021/ic400015v | Inorg. Chem. 2013, 52, 5138−5153

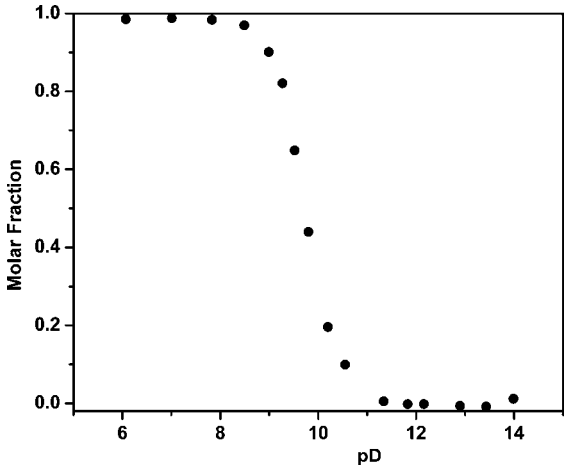

Figure 5. Molar fraction of H_2L1 as a function of pD.

thermodynamic stability constants were determined in aqueous solution, at T = 298.2 ± 0.1 K and 0.10 M ionic strength in $N(CH_3)_4NO_3$. Under these conditions, the kinetics of complex formation is very slow, and as a consequence the determinations were only possible using batch titrations after at least 15 days of stabilization. Once completely formed, the complexes are very inert to demetalation, see below. The obtained values are compiled in Table 3 and Table S3 of the Supporting Information together with those of related ligands for comparison.[38,41−43,50,51] The corresponding species distribution diagrams are shown in Figure 6 and in Figures S7−S9 for complexes of Cu^{2+}, Zn^{2+}, Al^{3+}, and Ga^{3+}, respectively.

Among the metal ions studied, only Cu^{2+}, Al^{3+}, and Ga^{3+} can form complexes under the mild conditions used, while the Zn^{2+} complex ([ZnL]) is formed in small amounts coexisting with $Zn(OH)_2$, see Figure S7 of the Supporting Information. The Ni^{2+}, Cd^{2+}, Pb^{2+}, and Gd^{3+} form complexes with both ligands in minor amounts, indicating that under the mild conditions used they could not be formed. However, only with Cu^{2+} are the two chelators able to form complexes in the entire pH range (see distribution diagrams in Figure 6), coexisting as a monoprotonated species $[CuHL]^+$ with free copper(II) at pH < 4, as [CuL] in the 6.0 to 7.5 pH region, and then the $[CuL(OH)]^-$ starts to be formed, which is the only species in solution at pH > 11. Faster complex formation is possible by preparing the solution at pH values > 7.5. Both ligands also form complexes with Al^{3+} and Ga^{3+} cations, at low pH, but they are not sufficiently strong to compete with the formation of the corresponding metal hydroxides, see Figures S8 and S9 of the Supporting Information. However, the $[GaL1]^+$ complex is the only species formed in the 3 to 5 pH region, and between about 5 and 7 pH values both ligands form stable species with Al^{3+} as AlL^+ or hydroxocomplexes.

When compared to nonbridged cyclen *N*-acetate derivatives, the stability constant values for the complexes of Cu^{2+}, Al^{3+}, and Ga^{3+} with the chelators studied here are very high, except for the Zn^{2+} ions (Table 3). However, stability constants are not the correct way to evaluate the metal complexation ability of ligands exhibiting different basicity. To take this effect into account, the pM values (−log [M]) were calculated at pH 7.4 (physiological) and presented in Table 4. The same information can be retrieved from apparent (or effective) constants determined at different pH values, see Figure S10.

Both chelators are selective for copper(II), while H_4dota, although exhibiting a slightly higher pCu value, is not selective for this metal ion as it forms complexes with similar strength with all the first transition divalent metal ions including Zn^{2+}, see Figure 7 and Figure S11 for H_2L2 and H_2do2a.[42,43] For Al^{3+} and Ga^{3+}, the three ligands present very similar pM values, and the distribution curves (Figures S8 and S9 of Supporting Information) indicate that at pH 7.4 the $[GaL1]^+$ and $[GaL2]^+$ complexes are almost completely dissociated, leaving in solution only gallium(III) hydroxides. For Al^{3+}, the studied chelators are slightly better than H_4dota existing at physiological pH in the form of hydroxocomplexes.

In conclusion, H_2L1 and H_2L2 are chelators exceptionally selective for Cu^{2+}, coordinating the other divalent metal ions (Mg^{2+}, Ca^{2+}, Ni^{2+}, Zn^{2+}, Cd^{2+}, and Pb^{2+}) with very low thermodynamic stability. For the trivalent Al^{3+} and Ga^{3+} cations, the stability constants with H_2L1 and H_2L2 are larger than for H_4dota (Tables 3 and 4) but not enough for it to be possible to use them at physiological pH in medical applications due to the strong tendency of these ions to form hydroxides, see Table 4. Another feature to stress is the crucial role on metal complexation of the acetate arms in H_2L1 and H_2L2. In fact, the parent compounds, L3 and L4, cannot form complexes

Table 3. Stepwise Stability Constants (K_{MH_iL}), in log units, for the Metal Complexes of H_2L1 and H_2L2 with Cu^{2+}, Zn^{2+}, Al^{3+}, and Ga^{3+} Metal Ions in Aqueous Solution (T = 298.2 K and I = 0.10 M in $N(CH_3)_4NO_3$)

equilibrium reaction[a]	H_2L1[b]	H_2L2[b]	cyclen[c]	H_2do2a[d]	H_4dota
$CuL + H^+ \rightleftarrows CuHL$	4.39	3.85		3.0	3.78[e]
$Cu^{2+} + L \rightleftarrows CuL$	23.25	20.87	23.4	21.1	22.25[e]
$CuLOH + H^+ \rightleftarrows CuL$	9.52	9.4			
$ZnL + H^+ \rightleftarrows ZnHL$				4.0	4.18[e]
$Zn^{2+} + L \rightleftarrows ZnL$	12.4	11.59	16.2	18.2	21.10[e]
$ZnLOH + H^+ \rightleftarrows ZnL$	9.5	8.4			
$AlL + H^+ \rightleftarrows AlHL$	3.47	4.5			
$Al^{3+} + L \rightleftarrows AlL$	20.17	18.3			17.0[f]
$AlLOH + H^+ \rightleftarrows AlL$	4.82	4.3			
$AlL(OH)_2 + H^+ \rightleftarrows AlLOH$	8.3	8.5			
$GaL + H^+ \rightleftarrows GaHL$					4.00[g]
$Ga^{3+} + L \rightleftarrows GaL$	25.08	21.6			21.33[g]

[a]Charges in the complex species were omitted, because they are different for the various ligands. [b]This work. [c]T = 298.2 K, I = 0.1 M in $NaNO_3$.[38] [d]T = 298.2 K, I = 0.1 M in $N(CH_2CH_3)_4NO_3$.[41] [e]T = 298.2 K, I = 0.1 M in $N(CH_3)_4NO_3$.[43] [f]T = 298.2 K, I = 0.20 M in $NaNO_3$.[50] [g]T = 298.2 K, I = 0.1 M in KCl.[51]

dx.doi.org/10.1021/ic400015v | Inorg. Chem. 2013, 52, 5138−5153

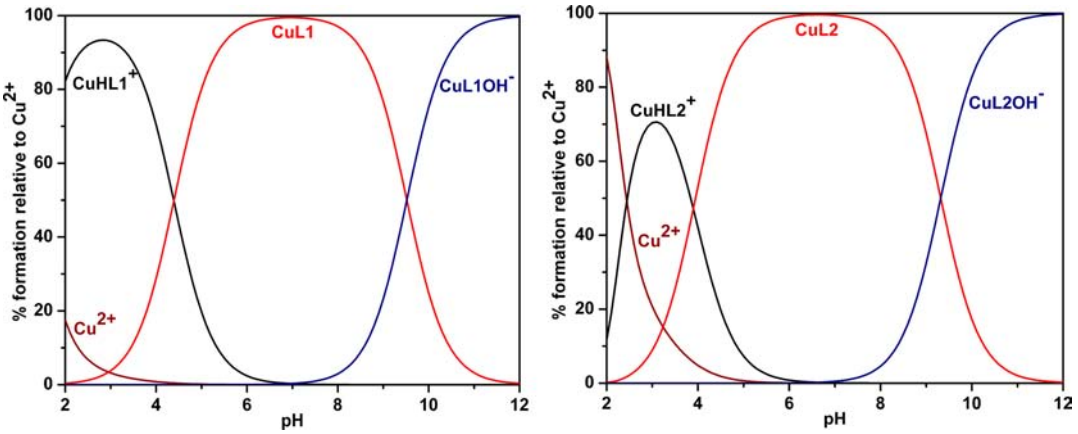

Figure 6. Species distribution diagrams for the complexes of Cu^{2+} with H_2L1 and H_2L2 in aqueous solution, $c_L = c_M = 1.0 \times 10^{-3}$ M.

Table 4. The pM[a] Values Calculated for Metal Complexes of the Discussed Ligands at pH 7.4

ion	H_2L1[b]	H_2L2[b]	cyclen[c]	H_2do2a[d]	H_4dota
pCu^{2+}	13.19	12.11	18.00	14.91	15.19[e]
pZn^{2+}	5.05	5.06	10.80	12.01	14.04[e]
pAl^{3+}	12.77	12.79			11.17[f]
pGa^{3+}	17.83	17.83			17.83[g]

[a]Values calculated for 100% molar excess of the ligand over the metal ion with $c_M = 1.00 \times 10^{-5}$ M, based on the protonation and stability constants of Tables S1 and S3 or in literature ones. [b]This work. [c]Ref 38. [d]Ref 41. [e]Refs 42 and 43. [f]Ref 50. [g]Ref 51.

with Cu^{2+} and Zn^{2+} at room temperature and aqueous solution as found by Bencini et al.[36] and by us in this work.

Structural Investigations. Single crystals of the compound $[Cu(H_2L1)](ClO_4)_2$ were obtained from slow evaporation of an aqueous solution of the complex in 5 $HClO_4$ M. The molecular structure is built up from a symmetric unit composed of one $[Cu(H_2L1)]^{2+}$ and two disordered ClO_4^- as counterions. The ORTEP view[52] of the structure of the $[Cu(H_2L1)]^{2+}$ complex cation with the labeling scheme adopted is depicted in Figure 8.

In Table 5 are given selected bond lengths and angles for the $[Cu(H_2L1)]^{2+}$ complex cation. The compound acts as a hexadentate ligand. The copper(II) center is in a distorted octahedral (O_h) environment bound to the four nitrogen atoms of the macrocycle, one oxygen atom from a carboxylic pendant arm and one oxygen from the dibenzofuran (DBF) unit. The octahedron is delimited by an equatorial plane, defined by the two nitrogen donor atoms [N(1), N(3)] and the two oxygen donor atoms [(O3), O(5)], and the compressed axial axis is defined by the nitrogen donor atoms [N(2), N(4)]. The short axial distance is in accordance with the EPR spectroscopic study (see below). The distances between the copper center and N(2), N(3), and N(4) nitrogen atoms, ranging from 2.005(5) to 2.089(2) Å, are typical of such interatomic distances reported in the International Tables for Crystallography [2.071(93) Å][53] or in the literature. The Cu−O(5) distance of 2.116(2) Å is shorter than the ones found in the literature for Cu−O(DBF) bonds, which is of 2.387(35) Å.[54,55] This is probably imposed by the strain of the ligand. In fact, a similar distance of 2.131(5) Å was reported for the structure of $[CuL3](PF_6)_2 \cdot CH_3CN$, recently published by Bazzicalupi et al.[36] The N−Cu−N and N−Cu−O(5) angles are close to the right angle value expected [86.11(2) to 93.7(8)°].

The distances C(10)−O(1) of 1.197(3) Å and C(12)−O(3) of 1.214(3) Å relative to the distances C(10)−O(2) of 1.332(3) Å and C(12)−O(4) of 1.320(3) Å confirm the carboxylic acid form of the COOH group.

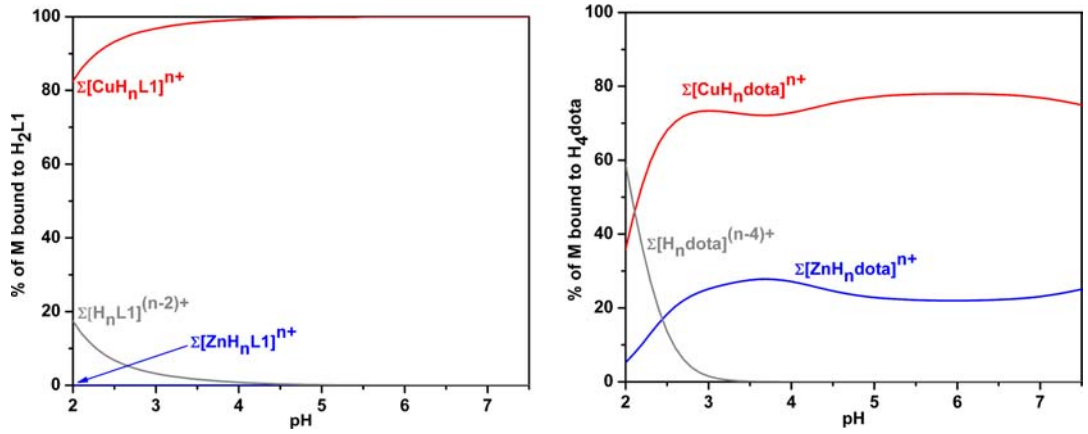

Figure 7. Species distribution diagrams for mixtures of Cu^{2+}, Zn^{2+}, and H_2L1 (left), and the same cations and H_4dota (right) in a 1:1:1 molar ratio and at a concentration of 1.0×10^{-3} M. The amounts of free ligands and metal complexes are expressed as the sum of all of their protonated species in percentage relative to the initial amount of H_2L1 or H_4dota.

dx.doi.org/10.1021/ic400015v | Inorg. Chem. 2013, 52, 5138−5153

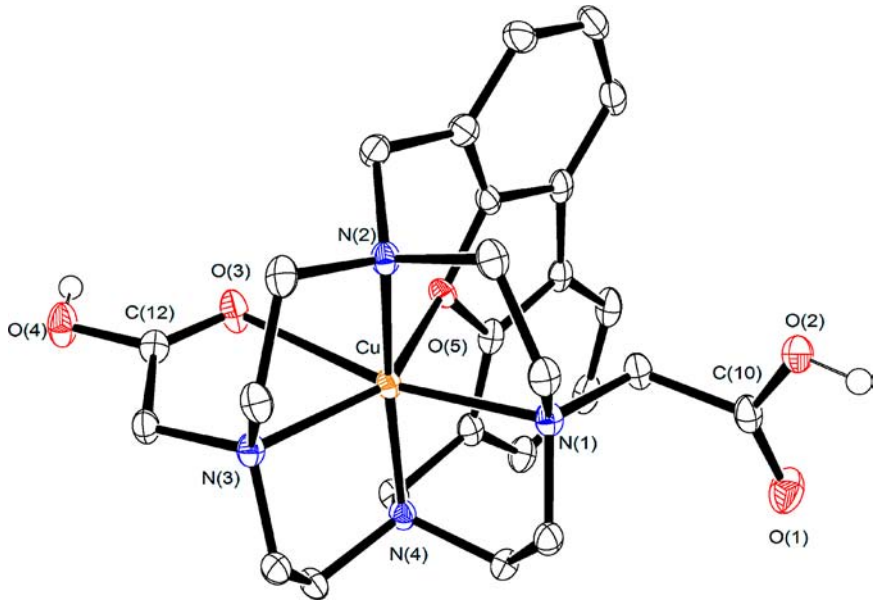

Figure 8. ORTEP view of $[Cu(H_2L1)]^{2+}$ showing thermal ellipsoids at the 50% probability level. Hydrogen atoms on carbon atoms and counterions have been omitted for clarity.

Table 5. Selected Bond Lengths (Å) and Angles (deg) of $[Cu(H_2L1)]^{2+}$ Complex Cation

bond lengths/Å		bond angles/deg	
Cu–N(1)	2.183(2)	N(1)–Cu–N(2)	86.36(8)
Cu–N(2)	2.005(2)	N(1)–Cu–N(3)	120.4(9)
Cu–N(3)	2.089(2)	N(1)–Cu–N(4)	86.11(9)
Cu–N(4)	2.010(2)	N(1)–Cu–O(5)	93.70(8)
Cu–O(5)	2.116(2)	N(2)–Cu–N(3)	89.46(9)
Cu–O(3)	2.557(2)	N(2)–Cu–N(4)	170.2(9)
C(10)–O(1)	1.197(3)	N(2)–Cu–O(3)	91.0(9)
C(10)–O(2)	1.332(3)	N(2)–Cu–O(5)	93.45(8)
C(12)–O(3)	1.214(3)	N(3)–Cu–N(4)	88.95(9)
C(12)–O(4)	1.320(3)	N(3)–Cu–O(3)	73.58(8)
		N(3)–Cu–O(5)	145.90(8)
		N(4)–Cu–O(3)	97.82(1)
		N(4)–Cu–O(5)	93.28(8)
		O(3)–Cu–O(5)	72.4(7)

Further details on the hydrogen bonds and crystal packing are available in the Supporting Information, Table S4 and Figures S12 and S13.

The molecular structure of the copper(II) complex of H_2L2 is built up from a symmetric unit composed of one [CuL2] and water molecules. The ORTEP view[52] of the structure of [CuL2] complex with the labeling scheme adopted is depicted in Figure 9, and in the Table 6 are given selected bond lengths and angles.

The compound acts as a pentadentate ligand in the solid state. The copper(II) center is in a trigonal bipyramid (D_{3h}) environment bound to the four nitrogen atoms of the macrocycle and one oxygen from the diphenyl ether (DPE) unit. The copper atom shares a plane with O(5), N(4), and N(1) atoms, which are in equatorial positions at about 120° angles to each other, and with N(2) and N(3) atoms above and below the plane, which are in apical positions. In fact, the trigonal distortion was calculated for the complex using the index structural parameter (τ) as previously defined by Addison et al.[56] The τ parameter assumes values of 0 and 1 for ideal square-pyramidal and trigonal-bipyramidal geometries, respectively. The τ value of 0.73 for [CuL2] is entirely consistent with a distorted trigonal bipyramid coordination sphere.

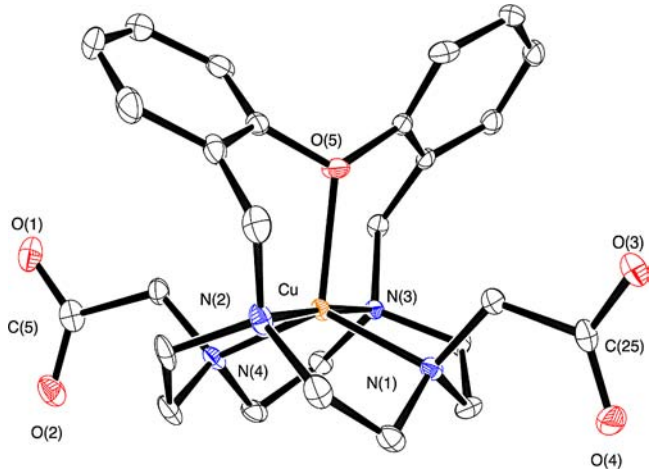

Figure 9. ORTEP view of [CuL2] showing thermal ellipsoids at the 50% probability level. Hydrogen atoms on carbon atoms and water molecules have been omitted for clarity.

Table 6. Selected Bond Lengths (Å) and Angles (deg) of [CuL2] Complex

bond lengths/Å		bond angles/deg	
Cu–N(1)	2.016(2)	N(3)–Cu–N(2)	176.12(8)
Cu–N(2)	2.003(2)	N(4)–Cu–O(5)	119.71(8)
Cu–N(3)	1.993(2)	N(4)–Cu–N(1)	132.27(8)
Cu–N(4)	2.013(2)	N(1)–Cu–O(5)	108.01(7)
Cu–O(5)	2.137(2)	N(2)–Cu–O(5)	91.85(8)
C(25)–O(3)	1.259(3)	N(2)–Cu–N(1)	88.53(8)
C(25)–O(4)	1.251(3)	N(2)–Cu–N(4)	89.22(8)
C(5)–O(1)	1.251(3)	N(3)–Cu–O(5)	91.96(7)
C(5)–O(2)	1.250(3)	N(3)–Cu–N(1)	89.66(8)
		N(3)–Cu–N(4)	89.46(8)

dx.doi.org/10.1021/ic400015v | Inorg. Chem. 2013, 52, 5138–5153

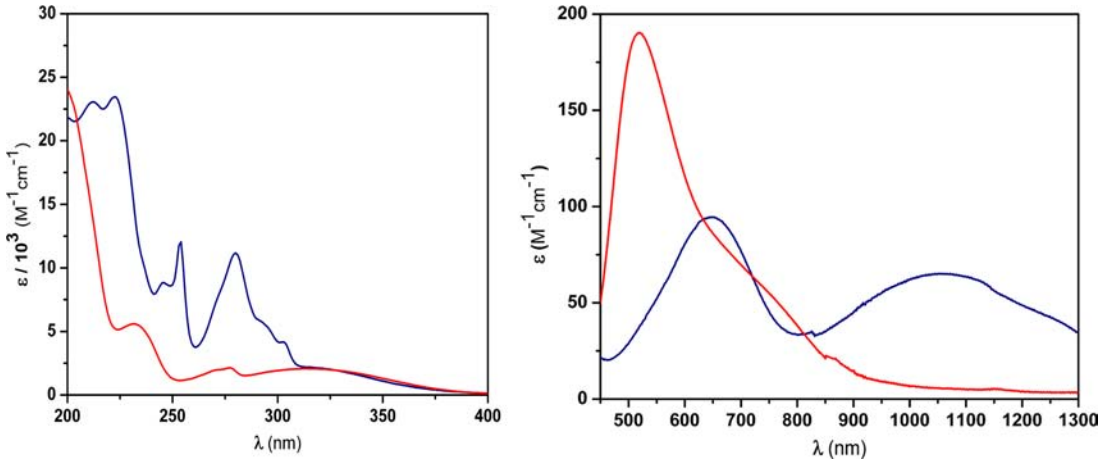

Figure 10. UV and vis−NIR spectra of [CuL1] (in blue) and [CuL2] (in red) in aqueous solution.

The distances between the copper center and N(1), N(2), N(3), and N(4) nitrogen atoms, ranging from 1.993(2) to 2.016(2) Å, are typical of such interatomic distances reported in the International Tables for Crystallography [2.071(93) Å][53] or in the literature. The Cu−O(5) distance of 2.137(2) Å is shorter than the ones found in the literature for Cu−O(ether) bonds, which is 2.371(96) Å, probably imposed by the strain of the ligand. A similar distance of 2.165(2) Å was reported for the corresponding distance in the structure of $[CuL4](ClO_4)_2$.[35]

Further details on the hydrogen bonds are available in the Supporting Information, Table S5.

UV−Vis−NIR and EPR Spectroscopic Studies of the Copper(II) Complexes of H_2L1 and H_2L2. UV−vis−NIR spectra were performed for [CuL1] and [CuL2] in aqueous solutions at pH 9.27 and 9.16, respectively (up to pH about 7, the spectra did not change). The [CuL1] complex exhibits a broad band in the visible region centered at λ = 650 nm (ε = 86 M^{-1} cm^{-1}) with a shoulder at higher energy (565 nm, 49 M^{-1} cm^{-1}), also a broad band in the NIR region (1051 nm, 57 M^{-1} cm^{-1}) and several bands in the UV region. The [CuL2] complex presents also a large band with λ_{max} = 520 nm (ε = 190 M^{-1} cm^{-1}) and a shoulder at 668 nm (80 M^{-1} cm^{-1}), no bands in the NIR region, and in the UV region exhibits only three main bands, see Figure 10 and Table S6. The bands in the vis−NIR region of both complexes, due to the copper d−d transitions, are quite different, indicating dissimilar geometries for the copper centers. The position and intensity of the bands rules out regular octahedral or tetragonal geometries.[57−60] However, especially for five and six coordination numbers, it is difficult to infer structural features from electronic spectra of copper(II) complexes as their stereochemistries vary over an appreciable range of distortion within a given coordination number, which is known as the plasticity effect.[60]

To go further in the characterization of the complexes, X-band EPR spectra of the same solutions were carried out at 90−298 K, and two of them are presented in Figure 11 together with the simulated ones. The spectra were obtained in a frozen water/ethylene glycol solution (1:1 v/v), although in H_2O they are similar, but in better resolution in the mixture of solvents. The EPR parameters obtained by simulation of the spectra of both complexes[61] are compiled in Table 7, together with the values for $[CuL3]^{2+}$ and $[CuL4]^{2+}$ under the same experimental conditions.

For [CuL1] complex, three different values of g were obtained, with $g_x > g_y \gg g_z \approx 2.00$, which is of the "inverted"

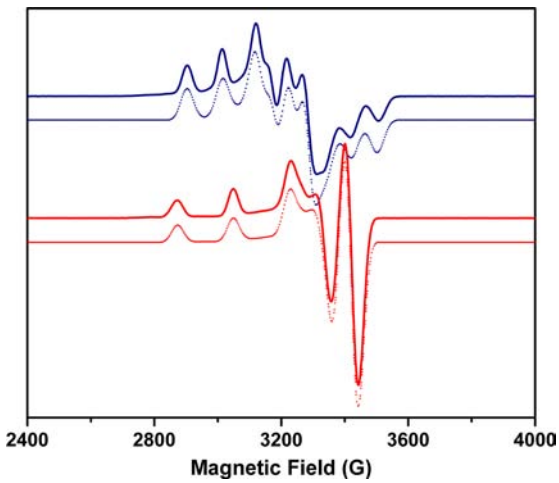

Figure 11. X-band EPR spectra of [CuL1] (in blue) and [CuL2] (in red) complexes in a frozen water/ethylene glycol solution (1:1 v/v) recorded at 90 K and the simulated ones (below the corresponding experimental spectra in dots). Experimental conditions: at pH 9.16 and concentration 2.70×10^{-3} M for [CuL1] and pH 9.27 and 2.66×10^{-3} M for [CuL2]. Microwave power of 2.0 mW, modulation amplitude of 1.0 mT, and the frequency (ν) was 9.68 GHz.

type. For these cases, the R parameter can be indicative of the predominance of the d_{z^2} or $d_{x^2-y^2}$ orbital in the ground state of the unpaired electron of the Cu^{2+} ion, $R = (g_y - g_z)/(g_x - g_y)$ with $g_x > g_y > g_z$. When $R > 1$, the greater contribution to the ground state arises from the d_{z^2} orbital, and when $R < 1$, the greater contribution to the ground state comes from the $d_{x^2-y^2}$ orbital.[62,63] The R value of 1.17 determined for [CuL1], as well as the values of the hyperfine splitting parameters, are indicative of a predominance of the d_{z^2} ground state, characteristic of axial-compressed geometries, such as distorted compressed octahedral or trigonal bipyramidal.[57−60,62−64] The data suggest the less common distorted compressed octahedral geometry, as also found in the crystal X-ray structure (see above). In spite of the compressed octahedral and trigonal bipyramidal geometries not being able to be distinguished in solution by their EPR spectra, they present very different vis−NIR spectra. In fact, the spectra of copper(II) in trigonal bipyramidal geometry are more intense then those of compressed octahedral one, but the latter present a NIR band almost of the same intensity as that of the vis region, as in the case of [CuL1].[58,64] The EPR spectra

dx.doi.org/10.1021/ic400015v | Inorg. Chem. 2013, 52, 5138−5153

Table 7. EPR Parameters for the Copper(II) Complexes of H_2L1 and H_2L2 at 90 K in Water/Ethylene Glycol Solution (1:1 v/v)[a]

complex	pH	λ_{max} (ε)[b]	EPR parameters						
			g_x	g_y	g_z	A_x[c]	A_y[c]	A_z[c]	R
[CuL1]	8.9	647 (76.0)	2.211	2.117	2.007	115.9	51.0	75.4	1.17
[CuL2]	9.2	520 (310.7)	2.03	2.05	2.162	3.0	24.5	177.0	0.18
$[CuL3]^{2+}$	7.9	585 (15)	2.03	2.058	2.176	2.4	46.8	194.5	0.24
$[CuL4]^{2+}$	7.7	501 (69)	2.03	2.06	2.161	30.2	29.6	204.2	0.25
$[Cu(cyclen)NO_3]^{+d}$		594 (271)	2.089		2.172	31.2		177.5	0

[a]Concentration of the complexes in the range 1.90×10^{-3} to 7.25×10^{-3} M. [b]λ_{max} of visible absorbance band in nm and ε_{mol} in M^{-1} cm^{-1}. [c]$A_i \times 10^4$ (cm^{-1}). [d]Values from refs 69 and 70.

recorded at several temperatures, starting at room temperature (297 K), showed no significant changes, indicating that the geometry around the copper is preserved, see Figure S14.

In contrast, for [CuL2] the values for the g parameter are $g_z > g_y \approx g_x$ and $g_x \geq 2.03$, characteristic of copper(II) complexes with slightly rhombic symmetry with elongation of the axial bonds and a $d_{x^2-y^2}$ ground state. Elongated rhombic-octahedral, tetragonal, distorted bicapped square pyramidal, or distorted square pyramidal symmetries would be consistent with these data.[57−60,64−67] On the other hand, the value of the maximum of the band in the visible and its large intensity point to square pyramidal geometries. The abnormally low value of g_z in [CuL2], when compared with the expected values of g_z versus A_z diagrams of Peisach and Blumberg,[68] can be explained by severe distortions of the N4 equatorial plane. Moreover, an increase of the g_z and a decrease of A_z parameters and simultaneously a red-shift of the d−d absorption band in the electronic spectra with coordination of axial ligands is expected.[64] However, the distortions of the Cu geometry in [CuL2] appear to be analogous to those of $[Cu(cyclen)(NO_3)](NO_3)$,[69−71] which adopts a square pyramidal geometry with one oxygen of the NO_3^- ligand in an axial position and the copper atom 0.5 Å above the plane containing the four N atoms of the macrocycle.[71] The observation of identical values for g_0 at 297 K ($g_0 = 2.088$ and $A_0 = 201.9 \times 10^{-4}$ cm^{-1}) and $\langle g \rangle$ at 90 K indicates that the solution coordination is not significantly temperature dependent (consistent with $g_0 = (g_x + g_y + g_z)/3$ and $A_0 = (A_x + A_y + A_z)/3$, see Figure S15). As seen above, in the single crystal X-ray structure, the copper center is also in a N_4O pentacoordinated environment, although adopting a trigonal pyramidal geometry.

Data of the electronic and EPR spectra of $[CuL3]^{2+}$ and $[CuL4]^{2+}$ under the same experimental conditions are also included in Tables 7 and S6. The complexes of both parent ligands present vis−NIR and EPR spectra in aqueous solution characteristic of copper(II) with elongation of the axial bonds, in a $d_{x^2-y^2}$ ground state and distorted N_4O square pyramidal geometry. The impact of the strain imposed by the backbone of the ligands is also observed for the complexes of the parent ligands, giving rise to smaller g_z values than expected. In the crystal X-ray structures of $[CuL3](PF_6)_2 \cdot CH_3CN$[36] and $[CuL4](ClO_4)_2$,[35] the copper is enclosed into the cavity of the macrobicycle bound to the five donor atoms, in a N_4O coordination sphere. In $[CuL4]^{2+}$, the copper center adopts a square pyramidal geometry where the four nitrogen atoms form the basal plane and the oxygen of the bridge takes the apical position, while in $[CuL3]^{2+}$ it displays an intermediate geometry between a square pyramid and a trigonal bipyramid one. In the last geometry, the apical positions are occupied by the two tertiary nitrogen atoms, and the equatorial plane is defined by the remaining secondary nitrogen atoms together with the oxygen of the bridge. In solution, the spectroscopic data revealed the copper center also in a N_4O square pyramidal environment for both $[CuL3]^{2+}$ and $[CuL4]^{2+}$ complexes, the $[CuL3]^{2+}$ exhibiting a stronger axial ligand field.

Although the spectroscopic data for [CuL2], $[CuL3]^{2+}$, and $[CuL4]^{2+}$ point in all cases to square pyramidal environments around the copper centers, the distortions from this geometry are more significant in [CuL2]. In spite of the similarities of geometries, in solution, between [CuL2] and $[CuL4]^{2+}$, the role of the H_2L2 arms in metal chelation is clearly observable. Indeed, L3 and L4 could not form metal complexes,[36] including with Cu^{2+}, under aqueous mild conditions. Trying to understand the role of the arms in H_2L1 and H_2L2 in metal chelation during the slow reactions of these chelators with Cu^{2+}, electronic, and EPR spectra were acquired along time. The results can be observed in Figures S16 and S17 for the vis and X-band EPR spectra, respectively. In the case of H_2L1 complexes, the sequence of spectra show the decrease of $[Cu(OH_2)_6]^{2+}$ and the increase of [CuL1] amounts, clearly indicating that the species formed since the beginning is the same as the final one, only the amount of complex formed increases with time. However, for the H_2L2 complex, a species with different geometry is formed in the first stages. In fact, the vis−NIR showed (see in Figure S18 the vis−NIR spectrum of the intermediate compound in more detail) one band at 630 nm with a shoulder at 520 nm and another larger band centered at 1030 nm. Along time, the band at 520 nm increases in intensity while that at 1030 nm decreases. In the final species, the band at 520 nm is the main one, while the first formed species exists in small percentage. The EPR spectra shown in Figure S17 supports the presence of one species with the copper center in the d_{z^2} ground state together with an increasing amount of the final species in the $d_{x^2-y^2}$ ground state. Additionally, the first spectra also revealed the presence of $[Cu(OH_2)_6]^{2+}$ that in the beginning is practically the only species in solution. It was not possible to obtain the completely pure complex corresponding to the d_{z^2} ground state, as it exists always with a certain amount of the final species; therefore the simulation of the spectra is not straightforward. However, all the data for this species are very similar to those obtained for [CuL1] (see in more detail one of the spectra with the corresponding simulation in Figure S19). The results clearly indicate that the intermediate copper(II) complex of H_2L2 corresponds also to a copper center in a hexacoordinate environment, of compressed octahedral symmetry, although the final stabilized complex point to a distorted square pyramidal geometry. These features suggest that the strain imposed by the H_2L2 backbone to the geometry of the copper(II) center is much more significant than that of H_2L1, preventing the direct

dx.doi.org/10.1021/ic400015v | Inorg. Chem. 2013, 52, 5138−5153

coordination of the acetate arms of the ligand in the stable form of the complex. Probably, the copper(II) complex of H_2L2 starts to be formed using one (or both) arm(s) on the coordination to the copper in a distorted compressed octahedral geometry, but the distortion to the usual geometries of the copper(II) imposed by the ligand led to a final rearrangement and to a square pyramidal environment, where the carboxylate groups are so distant that they cannot be considered bound to the copper center.

Kinetic Stability of [CuL1] and [CuL2] Complexes in Acidic Solution. The kinetic inertness of a complex to the dissociation can be more significant than its thermodynamic stability in the selection of ligands to form radiochelates to be used in medical applications.[72] The usual assay for evaluation of the kinetic inertness of a complex is its acid demetalation under pseudo-first-order conditions. It was found that acid inertness half-lives obtained under these conditions are useful first predictors for *in vivo* viability of ^{64}Cu-labeled chelates.[32] Therefore, the kinetic inertness of [CuL1] and [CuL2] was evaluated at 5 and 12 M HCl, respectively, in aqueous solution at several temperatures under *pseudo*-first-order conditions assayed by monitoring the υ_{max} absorbance in their visible spectra, see Figure S20 for the complex of H_2L1. The results are compiled in Table 8, which also includes the values for the most inert complexes of related ligands from the literature.[32,34,72] At 363.2 K and 5 M HCl, the half-life found for [CuL1] was 4.28 h. In 5 M $HClO_4$ at room temperature, the [CuL1] complex resists without decomposition for several weeks, at least the necessary time to grow crystals good enough for X-ray diffraction determination (see below). However, the [CuL2] complex is much more inert, and therefore 12 M HCl solutions and a temperature of 363.2 K were used. The half-life found is of 30.8 days, which is to the best of our knowledge the highest $t_{1/2}$ value reported until now for a copper(II) complex studied under such harsh conditions. Pandya et al. claim the same for the [Cu(c3b-te2a)] complex, although they only have a qualitative evaluation by HPLC.[34]

Table 8. Half-lives of the Dissociation of [CuL1] and [CuL2] in Very Harsh Conditions, and Values for the Most Kinetically Inert Copper(II) Complexes from the Literature

complex	conditions [HCl]/M (T/K)	half-life ($t_{1/2}$)	reference
[Cu(L1)]	5 (363.2)	4.28 h	this work
[Cu(L2)]	12 (363.2)	30.8 d	this work
[Cu(c3b-te2a)]	12 (363.2)	–[a]	34
[Cu(cb-te2a)]	5 (363.2)	6.4 d	72
[Cu(c3b-do2a)]	12 (363.2)	1.1 d	32
[Cu(cb-do2a)]	5 (303.2)	<2 m	72

[a]No $t_{1/2}$ values was reported; the authors mentioned that no sign of degradation was observed for up to seven days.

In conclusion, the copper(II) chelates studied in this work are extraordinarily inert, especially [CuL2]. This property together with their thermodynamic stability and selectivity point to them as potential candidates for radiopharmaceutical applications, especially [CuL2].

Electrochemical Behavior of the Copper(II) Complexes of H_2L1 and H_2L2. The efficacy of the copper radiopharmaceutical complex can also be limited by bioreduction followed by demetalation of the nonstabilized copper(I) complex. Therefore, the electrochemical behavior of the copper complexes needs also to be known. However, most polyazamacrocyclic complexes of copper(II) have rather negative reduction potentials that are well below the estimated −0.40 V (NHE) threshold for typical bioreductants.[4]

It was observed that cross-bridged cyclam copper(II) complexes typically exhibit *quasi*-reversible reductions but not those of cross-bridged cyclen ones, suggesting that the former macrobicycle can adapt somewhat to the coordination preferences of Cu(I).[72]

The cyclic voltammograms of the copper(II) complexes of H_2L1 and H_2L2 were carried out in aqueous solution at neutral pH, see Figure S21. The reductions of both complexes are irreversible with two cathodic waves at −652 and −784 mV (Ag/AgCl, scan rate 20 mV/s) for [CuL1] and −644 and −788 mV (Ag/AgCl, scan rate 20 mV/s) for [CuL2]. However, only one anodic peak on the reverse sweep was observed at −532 mV for [CuL1] and −584 mV for [CuL2]. This behavior is indicative of coupled chemical events. It seems that the reduced complexes may exist as mixtures of at least two species, which quickly equilibrate. It is curious to observe that the two species have inverse amounts in [CuL1] and [CuL2], see Figure S21b. These species may consist of four- and five-coordinate Cu^+ complexes, as also seen for other macrobicyclic complexes.[73,74] Therefore, H_2L1 and H_2L2 ligands, as all cyclen derivatives, due to their rigid backbones and the resulting very small cavity, do not appear to be able to adapt well to the coordination requirements of Cu^+ and stabilize it.

CONCLUSIONS

The effect of the presence of *trans*-diacetate arms on the acid–base behavior of the two cross-bridged compounds derived from cyclen with bridges composed of DBF and DPE moieties was evaluated, as well as on their metal complexes' properties. It was found that the acetate arms in H_2L1 and H_2L2 drastically and positively modify the coordination chemical behavior of the ligands compared to the parent ones, L3 and L4, leading to complexes thermodynamically more stable and kinetically more inert, especially their copper(II) complexes. Due to the cage formed by their backbones, these compounds are "proton sponges," and as a consequence, the complex formation is very slow. However, for the copper(II) complex this problem can be overcome forming the complexes at high pH or heating the solutions. Electronic and EPR spectroscopic data revealed that along the slow formation of [CuL1], the copper center always adopts a distorted compressed octahedral geometry, while in [CuL2] it adopts first an intermediate structure that is similar to the one of [CuL1] before the final stabilization in a structure with a square pyramidal environment around the copper center. In spite of the acetate arms probably not being involved in the stabilized copper(II) complex of H_2L2, they have a crucial importance in the formation and properties of the complex as revealed by the completely different behavior when compared with that of the parent ligand L4.

Although there are some other ligands forming copper(II) complexes with higher values of the stability constant, the studied compounds have constants that are high enough and very selective in the presence of the other biological metal ions. Additionally, they are extremely inert, especially [CuL2], placing them under especially good conditions for medical applications.

EXPERIMENTAL SECTION

Materials and Methods. Cyclen (1,4,7,10-tetraazacyclododecane) was obtained from CheMatech. All reagents obtained from commercial

dx.doi.org/10.1021/ic400015v | Inorg. Chem. 2013, 52, 5138–5153

sources were used as received. Organic solvents were dried by standard methods.[75] Elemental analyses and electrospray mass spectra (ESI-MS) were performed by the Analytical Services Unit of ITQB-UNL/IBET. The ^{1}H and $^{13}C\{^{1}H\}$ NMR spectra for the ligand characterization were recorded on two spectrometers, a Bruker Avance III 400 (^{1}H at 400.13 MHz and ^{13}C at 100.61 MHz) and on a Bruker Avance III 800 (^{1}H at 800.33 MHz and ^{13}C at 201.24 MHz), and the pH titration studies were recorded on a Bruker Avance DRX 300 spectrometer (^{1}H at 300.13 MHz) at a probe temperature of 298.2 K. Chemical shifts (δ) are given in parts per million and coupling constants (J) in hertz. The 3-(trimethylsilyl) propionic acid sodium salt was used as an internal reference for ^{1}H spectra in D_2O. The resonance assignments are based on peak integration and multiplicity, and on 2D homo- and heteronuclear correlation experiments.

Synthesis of Compound L3. A solution of dibenzofuran-4,6-dicarbaldehyde (2.88 g, 12.84 mmol) in 1,2-dichloroethane (40 cm^{-3}) was added dropwise to a stirred solution of 1,4,7,10-tetraazacyclododecane (cyclen; 2.21 g, 12.84 mmol) and fresh triacetoxyborohydride (7.61 g, 35.92 mmol) in 1,2-dichloroethane (250 cm^{-3}). The solution was stirred at room temperature under an atmosphere of nitrogen for 48 h. The reaction mixture was quenched by the addition of a 1 M NaOH aqueous solution (300 cm^{-3}), and the product was extracted with chloroform (3 × 200 cm^{-3}). The organic layer was dried over $MgSO_4$ and evaporated under reduced pressure. The crude product was washed with cyclohexane to give the compound L3 as a yellow powder (3.51 g, 75%). ^{1}H NMR (500 MHz, $CDCl_3$, 298 K): δ_H 2.50 (bs, 2 H), 2.53 (m, 8 H), 2.64 (m, 8 H), 4.00 (s, 4 H), 7.18 (m, 4 H), 7.79 (m, 2 H). ^{13}C NMR (125 MHz, $CDCl_3$, 298 K): δ_C 47.9, 53.0, 58.6, 120.9, 123.1, 124.4, 125.5, 128.7, 154.8. Elem. Anal. Calcd. for $C_{22}H_{28}N_4O$ (%): C, 72.50; H, 7.74; N, 15.37. Found: C, 72.3; H, 7.8; N, 15.3. MALDI-TOF (m/z): 364.9.

Synthesis of Compound H_2L1. The compound L3 was dissolved in MeCN (350 cm^{-3}), and K_2CO_3 (3.93 g, 28.52 mmol) and *tert*-butyl bromoacetate (2.78 g, 14.27 mmol) were then added. The reaction was heated to 40 °C for 4 h. After cooling, solids were removed by filtration, and the filtrate was evaporated under reduced pressure. Residual solvent was removed under high vacuum conditions, and the product was triturated with diethyl ether to give the compound as a yellow oil (2.19 g, 91%). ^{1}H NMR (600 MHz, $CDCl_3$, 323 K): δ_H 1.26 (s, 18 H), 2.68−2.71 (m, 4 H), 2.88−2.94 (m, 8 H), 3.01−3.05 (m, 4 H), 3.14−3.18 (m, 4 H), 4.67 (s, 4 H), 7.33 (t, 2 H, J = 7.5 Hz), 7.51 (d, 2 H, J = 7.5 Hz), 7.92 (d, 2 H, J = 7.5 Hz), 8.52 (br s, N^+−H). ^{13}C NMR (150 MHz, $CDCl_3$, 323 K): δ_C 27.9, 51.7, 51.8, 53.1, 57.8, 81.9, 119.6, 121.5, 123.7, 123.9, 128.9, 153.8, 168.8. ESI+ (m/z) 593.4 $(M + H)^+$; 537.3 $(M + H - {}^tBu)^+$.

The ester groups were hydrolyzed in concentrated hydrochloric acid (15 cm^{-3}). The reaction mixture was stirred at room temperature for 10 min. The hydrochloric acid was then evaporated off. The remaining oil was dissolved in acetone, and the desired product slowly precipitated. After removal of trace solvents under high vacuum conditions, L1(HBr)(HCl)·$2H_2O$ (1.487 g) was obtained as a white solid in a 67% yield. ^{1}H NMR (600 MHz, D_2O, 363 K, pD = 14): δ_H 2.52−2.56 (m, 5 H), 2.63−2.71 (m, 5 H), 2.98−3.02 (m, 5 H), 2.99−3.07 (m, 4 H), 3.12−3.17 (s, 4 H), 3.74 (s, 4 H), 7.31−7.32 (m, 2 H), 7.34−7.36 (m, 2 H), 7.90−7.92 (m, 2 H). Elem. Anal. Calcd. for $C_{26}H_{37}BrClN_4O_7$ (%): C, 49.26; H, 6.04; N, 8.84. Found: C, 49.60; H, 6.10; N, 8.93: ESI+ (m/z) 481.2 $(M + H)^+$; 503.2 $(M + Na)^+$.

Synthesis of Compound L4. The compound L4 was obtained from cyclen (0.78 g, 4.53 mmol) and bis(2-formylphenyl)ether (1.02 g, 4.53 mmol) in the presence of triacetoxyborohydride (2.69 g, 12.68 mmol) by using the same procedure reported for L3. The compound was isolated as a white powder (1.29 g, 78%). ^{1}H NMR (500 MHz, $CDCl_3$, 298 K): δ_H 2.05 (bs, 2 H), 2.45−2.82 (m, 16 H), 3.33 (d, 2 H, J = 12.5 Hz), 4.13 (d, 2 H, J = 12.5 Hz), 6.65 (m, 2 H), 6.96 (m, 2 H), 7.15 (m, 4 H). ^{13}C NMR (125 MHz, $CDCl_3$, 298 K): δ_C = 48.1, 48.4, 53.5, 55.9, 59.2, 119.3, 123.7, 130.0, 130.9, 132.5, 157.3. Elem. Anal. Calcd. for $C_{22}H_{30}N_4O$ (MW = 366.51) (%): C, 72.08; H, 8.26; N, 15.29. Found: C, 72.0; H, 8.3; N, 15.2. MALDI-TOF (m/z): 367.1.

Synthesis of Compound H_2L2. The compound L4 (1.0 g, 2.73 mmol) was dissolved in MeCN (150 cm^{3}). K_2CO_3 (1.51 g, 10.92 mmol) and tert-butyl bromoacetate (1.17 g, 6.01 mmol) were then added, and the reaction was heated to 40 °C for 4 h. After cooling, solids were removed by filtration, and the filtrate was evaporated under reduced pressure. Residual solvent was removed under high vacuum conditions, and the product was triturated with diethyl ether to give the compound as a yellow oil (1.20 g, 74%). ^{1}H NMR (600 MHz, $CDCl_3$, 298 K): δ_H 1.36 (s, 18 H), 2.74 (m, 4 H), 2.78−2.92 (m, 8 H), 2.98−3.24 (m, 8 H), 4.25 (s, 4 H), 6.78 (d, 2 H, J = 7.7 Hz), 7.14 (t, 2 H, J = 7.7 Hz), 7.29 (t, 2 H, J = 7.7 Hz), 7.60 (d, 2 H, J = 7.7 Hz), 8.55 (br s, N^+−H). ^{13}C NMR (150 MHz, $CDCl_3$, 298 K): δ_C 28.1, 47.9, 52.7, 54.4, 54.9, 81.7, 116.9, 124.1, 125.1, 130.6, 133.7, 154.7, 169.5. ESI-MS (m/z): 595.4 $(M + H)^+$.

The ester groups were hydrolyzed in concentrated hydrochloric acid (15 cm^3). The reaction mixture was stirred at room temperature for 10 min, and then the hydrochloric acid was evaporated, the remaining oil dissolved in acetone, and the desired product slowly precipitated. After removal of solvent traces under high vacuum conditions, L2(HBr)-(HCl)·0.5 H_2O (1.12 g) was obtained as a white solid in a 80% yield. ^{1}H NMR (600 MHz, D_2O, 363 K, pD = 14): δ_H 3.33 (s, 4 H), 3.37−3.41 (m, 4 H), 3.45−3.49 (m, 4 H), 3.54−3.60 (m, 8 H), 4.52 (s, 4 H), 7.47 (d, 2 H, J = 7.7 Hz), 7.86 (t, 2 H, J = 7.7 Hz), 8.06 (t, 2 H, J = 7.7 Hz), 8.08 (d, 2 H, J = 7.7 Hz). ^{13}C NMR (150 MHz, $CDCl_3$, 363 K): δ_C 48.6, 53.5, 55.7, 56.8, 118.0, 124.7, 126.4, 131.4, 133.9, 155.6, 179.2. Elem. Anal. Calcd. for $C_{26}H_{34}BrClN_4O_{5.5}$ (%): C, 51.07; H, 5.87; N, 9.12. Found: C, 51.28; H, 6.12; N, 9.20. ESI+ (m/z): 483.3 $(M + H)^+$.

Synthesis of [CuL1]. The compound H_2L1 (101 mg, 159 μmol) was dissolved in MeOH/H_2O 30:70 v/v (50 cm^3); then 0.95 equiv. of $Cu(ClO_4)_2$ was added and the pH raised to about 9 with aqueous KOH. The solution was heated at 60 °C for 2 h. After cooling the blue solution to room temperature, the pH observed was neutral and the solvent mixture was removed under vacuum conditions. Then, the complex was dissolved in MeOH, and the precipitate of perchlorate salts formed was removed. This was repeated until no precipitation occurred. Then, the MeOH was removed under vacuum conditions, and the blue powder of the complex obtained was dried (79 mg, 96.0%). Elem. Anal. Calcd. for $C_{26}H_{30}CuN_4O_5$ (%): C, 57.61; H, 5.58; N, 10.34. Found: C, 57.5; H, 5.56; N, 10.60.

A solution of the $[CuL1](ClO_4)_2\cdot(2H_2O)$ complex (2.00×10^{-3} M; 3.0 dm^{-3} in 5.0 M $HClO_4$ solution) was left to stand at room temperature. Single crystals in small sea-green prisms of $[Cu(H_2L1)](ClO_4)_2$ were obtained in about 15 days.

Synthesis of [CuL2]. A procedure similar to the one described for [CuL1] was used replacing the ligand with H_2L2 (100 mg, 162 μmol), yielding a purple powder of the desired complex that was dried under vacuum conditions (83 mg, 98.7%). Blue plate crystals of the complex were obtained after slow evaporation of water. Elem. Anal. Calcd. for $C_{26}H_{32}CuN_4O_5$ (%): C, 57.39; H, 5.93; N, 10.30. Found: C, 57.48; H, 6.18; N, 10.46.

X-Ray Crystallography. *Crystal Data for $[Cu(H_2L1)]^{2+}$.* $[C_{26}H_{32}CuN_4O_5]^{2+}$, $2[ClO_4]^-$, M = 743.00, monoclinic, space group $P2_{1/c}$, a = 9.9335(2) Å, b = 26.1852(6) Å, c = 14.6608(2) Å, β = 132.3410(10)°, V = 2818.69(9) Å^3, Z = 4, T = 115(2) K, D_c = 1.751 g.cm^{-3}, λ(Mo Kα) = 0.71073 Å, μ(Mo Kα) = 1.044 mm^{-3}, 12 278 reflections collected, 6438 unique. The maximum and minimum residual electron densities are 0.737 and −0.690 e Å^{-3}. The final agreement factors are $R(1)$ = 0.0440 and 0.0912, and $wR(2)$ = 0.0533 and 0.0966, for $I > 2\sigma(I)$ and all data, respectively.

Crystal Data for [CuL2]. $2(C_{26}H_{32}CuN_4O_5)$, $7(H_2O)$, M = 1214.30, monoclinic, space group $C2/c$, a = 9.6023(4) Å, b = 16.4735(6) Å, c = 33.8442(14) Å, β = 94.425(2)°, V = 5337.6(4) Å^3, Z = 4, T = 115(2) K, D_c = 1.511 g cm^{-3}, λ(Mo Kα) = 0.71073, μ(Mo Kα) = 0.878 mm^{-1}, 31 174 reflections collected, 6164 unique. The minimum and maximum residual electron densities are −0.439 and 0.513 e Å^{-3}. The final agreement factors are $R(1)$ = 0.0425 and 0.0789, and $wR(2)$ = 0.0779 and 0.0876, for $I > 2\sigma(I)$ and all data, respectively.

CCDC-907927 and CCDC-924316 contains the supplementary crystallographic data for this paper. These data can be obtained free of charge from The Cambridge Crystallographic Data Centre via www.ccdc.cam.ac.uk/data_request/cif.

dx.doi.org/10.1021/ic400015v | Inorg. Chem. 2013, 52, 5138−5153

X-Ray Equipment and Refinement. Diffraction data were collected on a Nonius Kappa Apex-II CCD diffractometer equipped with a nitrogen jet stream low-temperature system (Oxford Cryosystems). The X-ray source was graphite monochromated Mo Kα radiation (λ = 0.71073 Å) from a sealed tube. The lattice parameters were obtained by least-squares fit to the optimized setting angles of the entire set of collected reflections. No significant intensity decay or temperature drift was observed during the data collections. For $[Cu(H_2L1)]^{2+}$, data were reduced by using DENZO software[76] without applying absorption corrections; the missing absorption corrections were partially compensated by the data scaling procedure in the data reduction. The structure was solved by the charge flipping algorithm using the SUPERFLIP program.[77] For [CuL2], data were reduced by using SAINT V8.27B software[78] with applying multiscan absorption corrections. The structure was solved by using the SHELXS program.[79]

Refinements were carried out by full-matrix least-squares on F^2 using the SHELXL97 program[79] on the complete set of reflections. Anisotropic thermal parameters were used for non-hydrogen atoms. All H atoms, on carbon or oxygen atoms, were placed at calculated positions using a riding model with C−H = 0.95 Å (aromatic) or 0.99 Å (methylene) or O−H = 0.84 Å with $U_{iso}(H) = 1.2Ueq(CH_2)$, $U_{iso}(H) = 1.2U_{eq}(CH)$, or $U_{iso}(H) = 1.5Ueq(OH)$.

In $[Cu(H_2L1)](ClO_4)_2$, three oxygen atoms of each perchlorate anion exhibited disorder with the ratios 0.59(1)/0.41(1). The geometric parameters of minor disordered components in each group were restrained by using SAME restraints.[79] Similar U_{ij} constraints were applied within the disordered parts to maintain a reasonable model by using EADP constraints.[79]

Potentiometric Equipment and Work Conditions. The potentiometric setup for conventional titrations consisted of a 50 cm^3 glass-jacketed titration cell sealed from the atmosphere and connected to a separate glass-jacketed reference electrode cell by a Wilhelm type salt bridge containing 0.10 M $N(CH_3)_4NO_3$ solution. An Orion 720A+ measuring instrument fitted with a Metrohm 6.0123.100 glass electrode and an Orion 90−05−00 Ag/AgCl reference electrode was used for the measurements. The ionic strength of the experimental solutions was kept at 0.10 ± 0.01 M with $N(CH_3)_4NO_3$; temperature was controlled at 298.2 ± 0.1 K using Huber CC3-K6 compact cooling and heating bath thermostats and an Orion 91−70−06 ATC-probe previously calibrated. Atmospheric CO_2 was excluded from the titration cell during experiments by slightly bubbling purified nitrogen on the experimental solution. Titrant solutions were added through capillary tips at the surface of the experimental solution by a Metrohm Dosimat 665 automatic buret. The titration procedure is automatically controlled by software after the selection of suitable parameters, allowing for long unattended experimental runs. In cases where automatic titrations could not be preformed, out-of-cell titrations were carried out, and the electromotive force was measured with a Metrohm 6.0234.100 combined pH electrode previously calibrated.

Potentiometric Measurements. Purified water was obtained from a Millipore Milli-Q demineralization system. Stock solutions of H_2L1 and H_2L2 were prepared at *ca.* 2×10^{-3} M. The $N(CH_3)_4NO_3$ salt was prepared by neutralization of a commercial $N(CH_3)_4OH$ solution with HNO_3. Metal ion solutions were prepared in water at 0.025−0.050 M from analytical grade nitrate salts of the metal ions and standardized by titration with Na_2H_2edta.[80] Carbonate-free solutions of the titrant $N(CH_3)_4OH$ were obtained at *ca.* 0.10 M by treating freshly prepared Ag_2O with a solution of $N(CH_3)_4I$ under nitrogen. These solutions were standardized by application of Gran's method.[81] A 0.100 M standard solution of HNO_3 prepared from a commercial ampule was used for backtitrations. The $[H^+]$ of the solutions was determined by measurement of the electromotive force of the cell, $E = E^{o\prime} + Q \log[H^+] + E_j$. The term pH is defined as $-\log [H^+]$. $E^{o\prime}$ and Q were determined by titrating a solution of known hydrogen-ion concentration at the same ionic strength in the acid pH region. The liquid-junction potential, E_j, was found to be negligible under the experimental conditions used. The value of $K_w = [H^+][OH^-]$ was found to be equal to $10^{-13.80}$ by titrating a solution of known hydrogen-ion concentration at the same ionic strength in the alkaline pH region, considering $E^{o\prime}$ and Q valid for the entire pH range.

Measurements during conventional titrations were carried out with *ca.* 0.05 mmol of ligand in a total volume of *ca.* 30 cm^3, in the absence of metal ions and in the presence of each metal ion at 0.9:1 M/L ratio. A backtitration was always performed at the end of each direct complexation titration in order to check if equilibrium was attained throughout the full pH range. Each titration curve typically consisted of 50−60 points in the 2.5−11.5 pH range, and a minimum of two replicate titrations were performed for each system. In all cases, the direct and back-titration curves differ markedly, especially for the copper(II) ones of both ligands. In such cases, out-of-cell titrations were carried out.

Out-of-cell titrations (or batch titrations) for all systems of slow kinetics formation were carried out by preparation of independent vials of different pH values and under the experimental conditions used for the conventional titrations at about 3.00 cm^{-3} total volume. Each vial contains 3.00 cm^{-3} of the mother solution of the complex with the necessary amount of $N(CH_3)_4NO_3$ to control the ionic strength, and then the pH was adjusted at the desired value. A mother solution of the complex was prepared by addition of the ligand and metal ion in a 1:1 ratio, and the pH was adjusted at a value >7.5 by the addition of base ($N(CH_3)_4OH$) or acid (HNO_3) and used after 2−3 h of equilibration. The vials were tightly closed under nitrogen and kept at 298.2 K until the equilibrium was reached, which was controlled each week. For the complexes of both ligands, the equilibrium was generally reached after one week, and the vials were kept under the same conditions one additional week for control reasons.

NMR Spectroscopy. Two dimensional spectra were acquired on a Bruker Avance II 500 spectrometer (Bruker, Rheinstetten, Germany) working at a proton operating frequency of 500.43 MHz, equipped with a four channel 5 mm inverse detection probe head with pulse-field gradients along the z axis, or on a Bruker Avance III 800 spectrometer (Bruker, Rheinstetten, Germany) working at a proton operating frequency of 800.33 MHz, also equipped with a four channel 5 mm inverse detection probe head.

For the assignment strategy, spectra were run at 308.2 and 313.2 K using standard Bruker pulse programs. ^{13}C spectra were recorded at 125.76 MHz using the APT (attached proton test) sequence. The modulation of peak sign, to distinguish methyl and methyne from methylene signals, was achieved using a delay of 6.89 ms for the evolution of $^1J_{CH}$. Proton decoupling was applied during the acquisition stage using the WALTZ-16 sequence.[82] In the two-dimensional $^1H-^{13}C$ heteronuclear single quantum coherence (HSQC) spectra, a delay of 3.45 ms was used for evolution of $^1J_{CH}$, while in the heteronuclear multiple bond connectivity (HMBC) spectra a delay of 73.5 ms was used for the evolution of long-range couplings. In the HSQC, proton decoupling was achieved using the GARP4 sequence.[82]

For determination of the first two protonation constants of both ligands, ^1H NMR spectra in D_2O solution, at 6.5−14.5 pD range and 298.2 K, were recorded, *ca.* 20 points per titration. The ligand stock solutions were prepared at 0.010 M, and the titrant was a fresh CO_2-free KOD solution. The titrations were performed directly in the NMR tube, and the titrant was added with a research syringe (0.1−2.5 μL) and/or automatic pipettes (0−25 and 0−100 μL). The pH* was measured with an Orion 420A instrument fitted with a Hamilton Spintrode PN23819703 combined microelectrode after calibration with two buffers prepared in aqueous solution (pH 8.00 of borate/hydrochloric acid and pH 4.00 of citric acid/sodium hydroxide/sodium chloride). The final pD was calculated according to the equation pD = pH* + (0.40 ± 0.02),[48] where pH* corresponds to the reading of the pH meter. The measurements were carried out with *ca.* 0.05 mmol of each ligand in a total volume of 0.5 cm^3 without control of the ionic strength. The equilibrium constants in D_2O (K_D) were converted in H_2O (K_H) values using published equations.[48,49]

UV−Vis−NIR Measurements. Absorption spectra of the solutions studied were recorded from 200 to 900 nm at T = 298.2 ± 0.1 K using a UNICAM model UV-4 spectrophotometer, and from 850 to 1200

dx.doi.org/10.1021/ic400015v | Inorg. Chem. 2013, 52, 5138−5153

nm using a Shimadzu model UV-3100 spectrophotometer for NIR ranges.

For determination of the first protonation constant of both ligands, UV spectra of solutions of pH > 11.5 were recorded. The solutions were obtained by the addition of known amounts of KOH at 298.2 K, *ca.* 15 points per titration. Ligand stock solutions (7.0×10^{-5} M) and fresh CO_2-free KOH solutions as the titrant were prepared. The titration was carried out directly in the UV cell (with *ca.* 0.2 μmol of each ligand in a total volume of 3.0 cm^3, without control of the ionic strength), and the titrant was added with a Crison microBU 2031 buret.

Calculation of Thermodynamic Equilibrium Constants. The data from potentiometric titrations were used to determine the protonation constants of H_2L1 and H_2L2 (except the first one) and the stability constants with the different metal ions, while the ^{1}H NMR and UV-spectrophotometric titrations in the >6 pH region were used only to calculate the first two protonation constants of both compounds. The overall equilibrium constants β_i^H and $\beta_{M_mH_hL_l}$ (being $\beta_{M_mH_hL_l} = [M_mH_hL_l]/[M]_m[H]_h[L]_l$ and $\beta_{MH_{-1}L} = \beta_{ML(OH)} \times K_w$) were obtained by refinement of the potentiometric and spectrophotometric data with the HYPERQUAD program[83] and of the ^{1}H NMR data by the HYPNMR program.[84] Differences, in log units, between the values of protonated (or hydrolyzed) and nonprotonated constants provide the stepwise (log K) constants (being $K_{M_mH_hL_l} = [M_mH_hL_l]/[M_mH_{h-1}L_l][H]$). The errors quoted are the standard deviations of the overall stability constants calculated by the program when all the experimental data (at least two titration curves) for each system were fitted together. Species distribution diagrams were plotted from the calculated constants with the HYSS program.[44]

Kinetic Measurements. The dissociation kinetics of complexes of H_2L1 and H_2L2 with the Cu^{2+} ion in aqueous solution was followed as a function of time by absorption spectroscopy in the 400−850 nm region, using a UNICAM UV−vis spectrophotometer model UV-4, at 298.2 and 363.2 K. The spectra of [CuL1] were recorded each 15 min, and those of [CuL2] each 24 h until the complete disappearance of the band in the visible region. The solutions of the complexes were prepared, using $CuCl_2$ or $Cu(ClO_4)_2$, at 5.0×10^{-4} M in 5 M HCl (or 5 M $HClO_4$). The results were interpreted under pseudo-first-order conditions, and the half-life was calculated from the slope of linear ln(absorbance) vs time plots.

X-Band EPR Spectra. The EPR spectroscopic measurements were recorded with a Bruker EMX-8/2.7 spectrometer equipped with continuous-flow cryostat for liquid nitrogen operating at X-band. Room temperature (297 K) spectra were recorded on as-prepared solutions injected into a 1.6 mm inner diameter clear fused quartz cell to a height of approximately 10 mm. Solutions of the copper(II) complexes were prepared at 5.0×10^{-3} M. To these solutions ethylene glycol was added for the final 1:1 v/v H_2O/ethylene glycol ratio. The EPR spectra were recorded at a microwave power of 2.0 mW, frequency (ν) 9.67 GHz, T = 90−200 K and at room temperature, and were simulated using SpinCount software.[61]

Electrochemical Studies. A BAS CV-50W Voltammetric Analyzer connected to BAS/windows data acquisition software was used. Cyclic voltammetric experiments were performed in a glass cell MF-1082 from BAS in a C-2 cell enclosed in a Faraday cage, at room temperature, under nitrogen. The reference electrode was Ag/AgCl (MF-2052 from BAS) filled with 3 M NaCl in water, standardized for the redox couple $Fe(CN)_6^{3-}/Fe(CN)_6^{4-}$. The auxiliary electrode was a 7.5 cm platinum wire (MW-1032 from BAS) with a gold-plated connector. The working electrode was a glassy carbon (MF-2012 from BAS).

Copper(II) complexes of H_2L1 and H_2L2 ($\approx 6 \times 10^{-3}$ M; pH ≈ 7) were prepared in 0.10 M $N(CH_3)_4NO_3$ in water. The solutions were deaerated by a nitrogen stream prior to all measurements and were kept under nitrogen during the measurements. Between each scan, the working electrode was electrocleaned by multicycle scanning in the supporting electrolyte solution, polished on alumina 1 and 0.05 μm, cleaned with water, and sonicated before use, according to standard procedures.

Cyclic voltammograms with a sweep rate ranging from 10 to 200 mV s^{-1} were recorded in the region from +1.2 to −1.2 V. At this potential range the ligands were found to be electroinactive. The half-wave potentials, $E_{1/2}$, were obtained by averaging the anodic and cathodic peak potentials. All potential values are reported relative to the Ag/AgCl reference electrode, and the $E_{1/2}$ and ΔE_p of the $Fe(CN)_6^{3-}/Fe(CN)_6^{4-}$ couple, under our experimental conditions, were 196 mV and 73 mV, respectively.

■ ASSOCIATED CONTENT

Supporting Information

Tables of overall protonation and stability constants, of the assignment of ^{1}H and ^{13}C NMR resonances of H_2L1 and H_2L2 at basic pH; of UV−vis−NIR data of copper(II) complexes; HSQC and HMBC spectra of H_2L1 and H_2L2; representative speciation diagrams in solution; diagram of log K_{eff} as a function of the pH for several ligands; UV−vis spectra of the Cu^{2+} complexes; rate constants and time course for the acid-assisted dissociation of the Cu^{2+} complexes; voltammograms of copper(II) complexes. This material is available free of charge via the Internet at http://pubs.acs.org.

■ AUTHOR INFORMATION

Corresponding Author

*E-mail: delgado@itqb.unl.pt (R.D.), Franck.Denat@u-bourgogne.fr (F.D.).

Notes

The authors declare no competing financial interest.

■ ACKNOWLEDGMENTS

The authors acknowledge Fundação para a Ciência e a Tecnologia (FCT), with coparticipation of the European Community funds FEDER, POCI, QREN, and COMPETE for the financial support under project PTDC/QUI/67175/2006, including the fellowship of C.V.E. The NMR spectrometer used is part of the National NMR Network and was purchased in the framework of the National Program for Scientific Re-equipment, contract REDE/1517/RMN/2005, with funds from POCI 2010 (FEDER) and FCT. This work was also supported by FCT through grant #PEst-OE/EQB/LA0004/2011. Support was also provided by the CNRS, the University of Burgundy, and the Conseil Régional de Bourgogne through the 3MIM Project. P.D. thanks the French Ministry of Research for a Ph.D. grant.

■ REFERENCES

(1) Barefield, E. K. *Coord. Chem. Rev.* **2010**, *254*, 1607−1627.
(2) Timmons, J. C.; Hubin, T. J. *Coord. Chem. Rev.* **2010**, *254*, 1661−1685.
(3) Drewry, J. A.; Gunning, P. T. *Coord. Chem. Rev.* **2011**, *255*, 459−472.
(4) Wadas, T. J.; Wong, E. H.; Weisman, G. R.; Anderson, C. J. *Chem. Rev.* **2010**, *110*, 2858−2902.
(5) Mewis, R. E.; Archibald, S. J. *Coord. Chem. Rev.* **2010**, *254*, 1686−1712.
(6) Delgado, R.; Félix, V.; Lima, L. M. P.; Price, D. W. *Dalton Trans.* **2007**, 2734−2745.
(7) Suchý, M.; Hudson, R. H. E. *Eur. J. Org. Chem.* **2008**, 4847−4865.
(8) Merbach, A. E.; Tóth, É. *The Chemistry of Contrast Agents in Medical Magnetic Resonance Imaging*; John Wiley & Sons: Chichester, U. K., 2001.
(9) Bianchi, A.; Calabi, L.; Corana, F.; Fontana, S.; Losi, P.; Maiocchi, A.; Paleari, L.; Valtancoli, B. *Coord. Chem. Rev.* **2000**, *204*, 309−393.

(10) Caravan, P. *Acc. Chem. Res.* **2009**, *42*, 851−862.
(11) Kubíček, V.; Tóth, É. *Adv. Inorg. Chem.* **2009**, *61*, 63−129.
(12) Hermann, P.; Kotek, J.; Kubíček, V.; Lukeš, I. *Dalton Trans.* **2008**, 3027−3047.
(13) Liu, S. *Adv. Drug Delivery Rev.* **2008**, *60*, 1347−1370.
(14) Woods, M.; Kovacs, Z.; Sherry, A. D. *J. Supramol. Chem.* **2002**, *2*, 1−15.
(15) Liu, S.; Edwards, D. S. *Bioconjugate Chem.* **2001**, *12*, 7−34.
(16) Liu, S. *Chem. Soc. Rev.* **2004**, *33*, 445−461.
(17) Storr, T.; Thompson, K. H.; Orvig, C. *Chem. Soc. Rev.* **2006**, *35*, 534−544.
(18) Weisman, G. R.; Rogers, M. E.; Wong, E. H.; Jasinski, J. P.; Paight, E. S. *J. Am. Chem. Soc.* **1990**, *112*, 8604−8605.
(19) Weisman, G. R.; Wong, E. H.; Hill, D. C.; Rogers, M. E.; Reed, D. P.; Calabrese, J. C. *Chem. Commun.* **1996**, 947−948.
(20) Hubin, T. J.; McCormick, J. M.; Alcock, N. W.; Busch, D. H. *Inorg. Chem.* **1998**, *37*, 6549−6551.
(21) Wong, E. H.; Weisman, G. R.; Hill, D. C.; Reed, D. P.; Rogers, M. E.; Condon, J. S.; Fagan, M. A.; Calabrese, J. C.; Lam, K.-C.; Guzei, I. A.; Rheingold, A. L. *J. Am. Chem. Soc.* **2000**, *122*, 10561−10572.
(22) Hubin, T. J.; Alcock, N. W.; Seib, L. L.; Busch, D. H. *Inorg. Chem.* **2002**, *41*, 7006−7014.
(23) Bencini, A.; Bianchi, A.; Bazzicallupi, C.; Ciampolini, M.; Fusi, V.; Micheloni, M.; Nardi, N.; Paoli, P.; Valtancoli, P. *Supramol. Chem.* **1994**, *3*, 141−146.
(24) Niu, W.; Wong, E. H.; Weisman, G. R.; Hill, D. C.; Tranchemontagne, D.; Lam, K.-C.; Sommer, R. D.; Zakharov, L. N.; Rheingold, A. L. *Dalton Trans.* **2004**, 3536−3547.
(25) Bencini, A.; Biagini, S.; Giorgi, C.; Handel, H.; Le Baccon, M.; Mariani, P.; Paoletti, P.; Rossi, P.; Tripier, R.; Valtancoli, B. *Eur. J. Org. Chem.* **2009**, *32*, 5610−5621.
(26) Springborg, J. *Dalton Trans.* **2003**, 1653−1665.
(27) Boswell, C. A.; Regino, C. A. S.; Baidoo, K. E.; Wong, K. J.; Bumb, A.; Xu, H.; Milenic, D. E.; Kelly, J. A.; Lai, C. C.; Brechbiel, M. W. *Bioconjugate Chem.* **2008**, *19*, 1476−1484.
(28) Sun, X.; Wuest, M.; Weisman, G. R.; Wong, E. H.; Reed, D. P.; Boswell, C. A.; Motekaitis, R.; Martell, A. E.; Welch, M. J.; Anderson, C. J. *J. Med. Chem.* **2002**, *45*, 469−477.
(29) Sprague, J. E.; Peng, Y.; Fiamengo, A. L.; Woodin, K. S.; Southwick, E. A.; Weisman, G. R.; Wong, E. H.; Golen, J. A.; Rheingold, A. L.; Anderson, C. J. *J. Med. Chem.* **2007**, *50*, 2527−2535.
(30) Boswell, C. A.; Sun, X.; Niu, W.; Weisman, G. R.; Wong, E. H.; Rheingold, A. L.; Anderson, C. J. *J. Med. Chem.* **2004**, *47*, 1465−1474.
(31) Stigers, D. J.; Ferdani, R.; Weisman, G. R.; Wong, E. H.; Anderson, C. J.; Golen, J. A.; Moore, C.; Rheingold, A. L. *Dalton Trans.* **2010**, *39*, 1699−1701.
(32) Odendaal, Y.; Fiamengo, A. L.; Ferdani, R.; Wadas, T. J.; Hill, D. C.; Peng, Y.; Heroux, K. J.; Golen, J. A.; Rheingold, A. L.; Anderson, C. J.; Weisman, G. R.; Wong, E. H. *Inorg. Chem.* **2011**, *50*, 3078−3086.
(33) Ferdani, R.; Stigers, D. J.; Fiamengo, A. L.; Wei, L.; Li, B. T. Y.; Golen, J. A.; Rheingold, A. L.; Weisman, G. R.; Wong, E. H.; Anderson, C. J. *Dalton Trans.* **2012**, *41*, 1938−1950.
(34) Pandya, D. N.; Dale, A. V.; Kim, J. Y.; Lee, H.; Ha, Y. S.; Il An, G.; Yoo, J. *Bioconjugate Chem.* **2012**, *23*, 330−335.
(35) Chaux, F.; Denat, F.; Espinosa, E.; Guilard, R. *Chem. Commun.* **2006**, 5054−5056.
(36) Bazzicalupi, C.; Bencini, A.; Ciattini, S.; Denat, F.; Désogère, P.; Goze, C.; Matera, I.; Valtancoli, B. *Dalton Trans.* **2010**, *39*, 11643−11653.
(37) Ruangpornvisuti, V. W.; Probst, M. M.; Rode, B. M. *Inorg. Chim. Acta* **1988**, *144*, 21−23.
(38) Hancock, R. D.; Shaikjee, M. S.; Dobson, S. M.; Boeyens, J. C. A. *Inorg. Chim. Acta* **1988**, *154*, 229−238.
(39) Koike, R. T.; Kajitani, S.; Nakamura, I.; Kimura, E.; Shiro, M. *J. Am. Chem. Soc.* **1995**, *117*, 1210−1219.
(40) Desreux, J. F.; Merciny, E.; Loncin, M. F. *Inorg. Chem.* **1981**, *20*, 987−991.
(41) Weeks, J. M.; Taylor, M. R.; Wainwright, K. P. *J. Chem. Soc., Dalton Trans.* **1997**, 317−322.
(42) Delgado, R.; Fraústo da Silva, J. J. R. *Talanta* **1982**, *29*, 815−822.
(43) Chaves, S.; Delgado, R.; Fraústo da Silva, J.J. R. *Talanta* **1992**, *39*, 249−254.
(44) Alderighi, L.; Gans, P.; Ienco, A.; Peters, D.; Sabatini, A.; Vacca, A. *Coord. Chem. Rev.* **1999**, *184*, 311−318.
(45) Bernier, N.; Costa, J.; Delgado, R.; Félix, V.; Royal, G.; Tripier, R. *Dalton Trans.* **2011**, *40*, 4514−4526 and references therein.
(46) Bencini, A.; Bianchi, A.; García-España, E.; Micheloni, M.; Ramirez, J. A. *Coord. Chem. Rev.* **1999**, *188*, 97−156.
(47) Amorim, M. T. S.; Ascenso, J. R.; Delgado, R.; Fraústo da Silva, J. J. R. *J. Chem. Soc., Dalton Trans.* **1990**, 3449−3455.
(48) Delgado, R.; Fraústo da Silva, J. J. R.; Amorim, M. T. S.; Cabral, M. F.; Chaves, S.; Costa, J. *Anal. Chim. Acta* **1991**, *245*, 271−282.
(49) Krężel, A.; Bal, W. *J. Inorg. Biochem.* **2004**, *98*, 161−166.
(50) Kodama, M.; Kimura, E. *Bull. Chem. Soc. Jpn.* **1995**, *68*, 852−857.
(51) Clarke, E. T.; Martell, A. E. *Inorg. Chim. Acta* **1991**, *190*, 37−46.
(52) Farrugia, L. *J. Appl. Crystallogr.* **1997**, *30*, 565.
(53) Wilson, A. J. C.; Prince, E. *International Tables for Crystallography: Mathematical, Physical and Chemical Tables*, Kluwer Academic: Dordrecht, The Netherlands, 1999; Vol. *C*.
(54) Li, F.; Delgado, R.; Coelho, A.; Drew, M. G. B.; Félix, V. *Tetrahedron* **2006**, *62*, 8550−8558.
(55) Li, F.; Li, L.; Delgado, R.; Drew, M. G. B.; Félix, V. *Dalton Trans.* **2007**, 1316−1324.
(56) Addison, A. W.; Rao, T. N.; Reedijk, J.; van Rijn, J.; Verschoor, G. C. *J. Chem. Soc., Dalton Trans.* **1984**, 1349−1356.
(57) Hathaway, B. J.; Tomlinson, A. A. G. *Coord. Chem. Rev.* **1970**, *5*, 1−43.
(58) Hathaway, B. J.; Billing, D. E. *Coord. Chem. Rev.* **1970**, *5*, 143−207.
(59) Lever, A. B. P. *Inorganic Electronic Spectroscopy*, 2nd ed.; Elsevier: Amsterdam, 1984; pp 554−572.
(60) Hathaway, B. J. *Coord. Chem. Rev.* **1983**, *52*, 87−169.
(61) Hendrich, M. P. *SpinCount software*; Carnegie Mellon University: Pittsburgh, PA. SpinCount is available at http://www.chem.cmu.edu/groups/hendrich/.
(62) Garribba, E.; Micera, G. *J. Chem. Educ.* **2006**, *83*, 1229−1232.
(63) Halcrow, M. A. *Dalton Trans.* **2003**, 4375−4384.
(64) Valko, M.; Morris, H.; Mazúr, M.; Telser, J.; McInnes, E. J. L.; Mabbs, F. E. *J. Phys. Chem. B* **1999**, *103*, 5591−5597.
(65) Billing, D. E.; Hathaway, B. J. *J. Chem. Soc. A* **1969**, 1516−1519.
(66) Lommens, P.; Feys, J.; Vrielinck, H.; De Buysser, K.; Herman, G.; Callens, F.; Van Driessche, I. *Dalton Trans.* **2012**, *41*, 3574−3582.
(67) Rakhit, G.; Sarkar, B. *J. Inorg. Biochem.* **1981**, *15*, 233−241.
(68) Peisach, J.; Blumberg, W. E. *Arch. Biochem. Biophys.* **1974**, *165*, 691−708.
(69) Styka, M. C.; Smierciak, R. C.; Blinn, E. L.; DeSimone, R. E.; Passariello, J. V. *Inorg. Chem.* **1978**, *17*, 82−86.
(70) Miyoshi, K.; Tanaka, H.; Kimura, E.; Tsuboyama, S.; Murata, S.; Shimizu, H.; Ishizu, K. *Inorg. Chim. Acta* **1983**, *78*, 23−30.
(71) Clay, R.; Murray-Rust, P.; Murray-Rust, J. *Acta Crystallogr.* **1979**, *B35*, 1894−1895.
(72) Woodin, K. S.; Heroux, K. J.; Boswell, C. A.; Wong, E. H.; Weisman, G. R.; Niu, W.; Tomellini, S. A.; Anderson, C. J.; Zakharov, L. N.; Rheingold, A. L. *Eur. J. Inorg. Chem.* **2005**, 4829−4833.
(73) Bell, C. A.; Bernhardt, P. V.; Gahan, L. R.; Martínez, M.; Monteiro, M. J.; Rodríguez, C.; Sharrad, C. A. *Chem.—Eur. J.* **2010**, *16*, 3166−3175.
(74) Hubin, T. J.; Alcock, N. W.; Morton, M. D.; Busch, D. H. *Inorg. Chim. Acta* **2003**, *348*, 33−40.
(75) Perrin, D. D.; Armarego, W. L. F. *Purification of Laboratory Chemicals*, 3rd ed.; Pergamon: Oxford, U. K., 1988.
(76) Otwinowski, Z.; Minor, W. *Methods in Enzymology* **1997**, *276*, 307−326.
(77) Palatinus, L.; Chapuis, G. *J. Appl. Crystallogr.* **2007**, *40*, 786−790.
(78) *SAINT*; Bruker: Madison, WI, 2012.

(79) Sheldrick, G. M. *Acta Crystallogr., Sect. A* **2008**, *64*, 112−122.
(80) Schwarzenbach, G.; Flaschka, W. *Complexometric Titrations*; Methuen & Co: London, 1969.
(81) Rossotti, J. J.; Rossotti, H. J. *J. Chem. Educ.* **1965**, *42*, 375−378.
(82) Shaka, A. J.; Keeler, J.; Frenkiel, T.; Freeman, R. *J. Magn. Reson.* **1983**, *52*, 335−338.
(83) Gans, P.; Sabatini, A.; Vacca, A. *Talanta* **1996**, *43*, 1739−1753.
(84) Frassineti, C.; Ghelli, S.; Gans, P.; Sabatini, A.; Moruzzi, M. S.; Vacca, A. *Anal. Biochem.* **1995**, *231*, 374−382.

dx.doi.org/10.1021/ic400015v | *Inorg. Chem.* 2013, 52, 5138−5153